Journal of Chromatography, 384 (1987) 45–79
Elsevier Science Publishers B.V., Amsterdam — Printed in The Netherlands

CHROMSYMP. 970

SIMPLIFIED DESCRIPTION OF HIGH-PERFORMANCE LIQUID CHROMATOGRAPHIC SEPARATION UNDER OVERLOAD CONDITIONS, BASED ON THE CRAIG DISTRIBUTION MODEL

II. EFFECT OF ISOTHERM TYPE, AND EXPERIMENTAL VERIFICATION OF COMPUTER SIMULATIONS FOR A SINGLE BAND

J. E. EBLE and R. L. GROB
Chemistry Department, Villanova University, Villanova, PA 19085 (U.S.A.)
P. E. ANTLE
Biomedical Products Department, E. I. Du Pont de Nemours & Co., Concord Plaza, Wilmington, DE 19898 (U.S.A.)
and
L. R. SNYDER*
LC Resources, Inc., 26 Silverwood Court, Orinda, CA 94563 (U.S.A.)

SUMMARY

The preparative high-performance liquid chromatography (HPLC) model described in the preceding paper has been tested for nine different solute–column combinations under reversed-phase overload conditions. Following certain empirical adjustments of the model, good agreement between experimental and predicted elution curves was observed. One such adjustment relates to the value of the column saturation capacity w_s. This value can be obtained either from isotherm data or from separations under overload conditions. In some cases these two w_s values agree, but in other cases they differ by factors of almost 100. The latter situation appears due to strong retention of solute molecules on silanol sites, rather than on the non-polar bonded phase. Use of chromatographically derived values of w_s leads to accurate predictions of the elution band as a function of sample size.

Minor adjustments were also required in the shapes of the k'/k_0 *vs.* w_{xk} and N/N_0 *vs.* w_{xN} plots predicted by Craig simulations. Finally, it was found that in every case "real" columns are more quickly overloaded with respect to N than is predicted by Craig simulation. The value of w_s that can be inferred from k' overloading must be decreased by a factor of about 2.5 to account for the dependence of N on sample size. With these modifications of the model, it appears possible to accurately predict the elution curves for most HPLC systems as a function of sample size.

INTRODUCTION

In the preceding paper[1] a simple approach for understanding high-perform-

0021-9673/87/$03.50

ance liquid chromatographic (HPLC) separations under overload conditions was described. That study began with Craig simulations of HPLC separations as a function of (a) sample size w_x, (b) the maximum ("saturation") capacity of the column for sample w_s, and (c) the plate number N_0 and capacity factor k_0 measured for a small sample. It was then shown that the concentration-time profile of a single elution band (from Craig simulations) can be predicted as a function of w_x/w_s, k_0 and N_0, using a simplified (faster) computer simulation. The latter was referred to as a "model simulation", in contrast to the original approach ("Craig simulation"). These Craig simulations and derived correlations for the model simulations are so far based on Langmuir isotherms.

"Real" HPLC systems do not often meet all the requirements of Langmuir-isotherm sorption. It is therefore of interest to examine how our model will be affected in practice by such deviations from "ideal" behavior. The present paper addresses this question. We also report experimental data that verify our model for HPLC systems that involve the overload separation of a single solute. The present studies provide a basis for the corresponding interpretation and prediction of separations involving two or more co-eluting solutes. We will report on this in following papers.

THEORY

Non-Langmuir isotherms

The Langmuir isotherm is a good starting point for an understanding of the general characteristics of HPLC separation under overload conditions. Many experimental systems appear to exhibit Langmuir sorption, and most HPLC separations show a decrease in retention and plate number plus increase in band-tailing with increasing sample size, as predicted by the Langmuir isotherm. However in most cases the Langmuir isotherm is only an approximation of actual sorption data. Three separate effects can contribute to non-Langmuir behavior:

(i) Heterogeneity of the sorption surface and/or "localization" effects, such that the sorption of solute at low surface coverages is more favorable than at high coverages; a simple case is a two-site stationary phase, where sample molecules are retained strongly by one kind of site and weakly by the other;

(ii) non-unity stoichiometry of the retention process; the Langmuir isotherm assumes a one-to-one displacement process of the form

$$X_m + M_s \rightleftharpoons X_s + M_m \tag{1}$$

for a solute molecule X and mobile phase molecule M, in stationary (s) or mobile (m) phases. However, a more general possibility is

$$X_m + nM_s \rightleftharpoons X_s + nM_m \tag{2}$$

where $n > 1$. This might correspond to the displacement of n small molecules of mobile phase by a single large solute molecule;

(iii) solute–solute interactions that alter the free energy of sorption for high solute concentrations in the mobile or stationary phase.

A discussion of these effects for the case of liquid–solid (adsorption) chro-

matography is given in refs. 2–4. For the general case, a complete theoretical description of real isotherms will be quite complex; such a treatment is not readily adaptable to practical application in preparative separations. Here, we will examine certain general features of non-Langmuir adsorption with reference to our model for overload HPLC. We will see that many non-Langmuir systems yield isotherms that closely resemble the Langmuir isotherm over a certain range of solute concentrations. This means that our present model[1] can still provide a good description of the resulting elution band.

Heterogeneous stationary phases and solute localization

These effects have been discussed by several workers[2–6] for silica or alumina as adsorbents (liquid–solid chromatography). Stationary phase heterogeneity refers to the presence on the adsorbent surface of different kinds of adsorption sites or sites of differing energy. As a result, solute molecules will adsorb onto the stronger sites first, before filling the weaker sites. Solute localization refers to the attachment of solute molecules to specific sites, so that the solute occupies a narrowly defined position on the adsorbent surface. When a certain fraction of the surface is covered by adsorbed (and localized) solute molecules, further filling of the adsorbed monolayer is energetically less favorable. Either access to the surface is restricted by steric crowding of already adsorbed molecules, or proper positioning of the adsorbate for localized adsorption becomes impossible. These two effects, site heterogeneity and solute localization, have often been confused or lumped together.

Site heterogeneity. Consider the simplest such case, an adsorbent with sites of two different kinds. This frequently arises in the reversed-phase HPLC of polar or ionic solutes, which can interact either with the non-polar bonded phase or with unreacted silanol groups. We can describe the resulting isotherm as the sum of two separate isotherms, one for each set of sites. Let the column capacity w_s for adsorption onto sites of the first kind (i) be w_{s1}, and let the column capacity for the second set of sites (2) be w_{s2}. Similarly, let the solute mass w_{xs} in the stationary phase be w_1 for sites of the first type, and w_2 for sites of the second type. Let the value of k_0 for the first group of sites be k_1, and for the second group k_2. From eqn. 2 of the preceding paper[1] we know that the equilibrium uptake of solute (w_1 or w_2) by the adsorbent is equal to

$$\text{(sites 1)} \quad 1/w_1 = a_1 + b_1/C_x \tag{3}$$

and

$$\text{(sites 2)} \quad 1/w_2 = a_2 + b_2/C_x \tag{4}$$

The quantities a_1 and a_2 are equal to $1/w_{s1}$ and $1/w_{s2}$, respectively. Similarly, b_1 and b_2 are equal to $1/(V_m k_1)$ and $1/(V_m k_2)$, respectively. The combined uptake of solute by the column is

$$w_{xs} = w_1 + w_2 \tag{5}$$

Consequently we can calculate the composite isotherm from a knowledge of the individual isotherms.

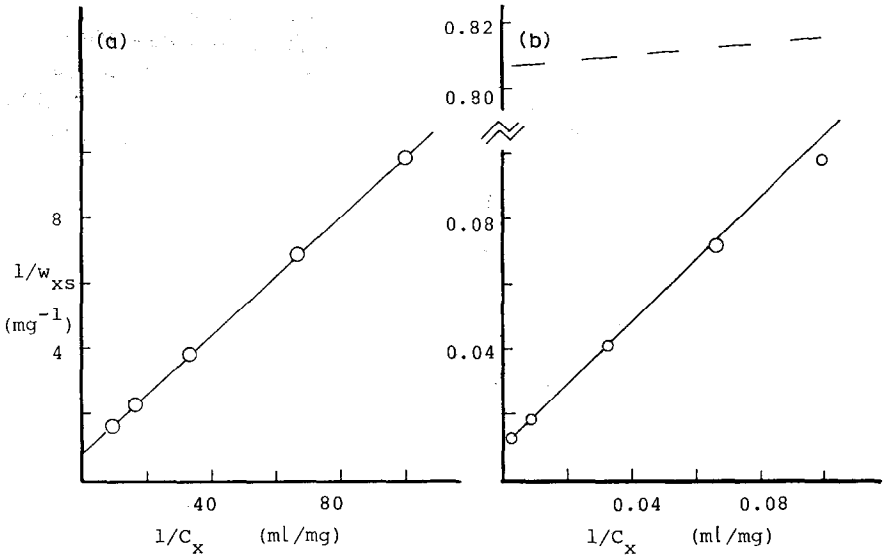

Fig. 1. Calculated isotherm for a two-site surface (site heterogeneity). $w_{s1} = 1$ mg, $w_{s2} = 100$ mg, $V_m k_1 = 10$, $V_m k_2 = 1$. (a) Data for low values of C_x; (b) data for high values of C_x.

When the values of k_0 for the two kinds of sites (k_1 and k_2) are sufficiently different, plots of $1/w_{xs}$ *vs.* $1/C_x$ become bimodal, each part corresponding roughly to the isotherm for a given set of sites. This is illustrated in Fig. 1, for a hypothetical case that is representative of many real HPLC systems: sites 1 are quite strong, but present in small concentration; sites 2 are much weaker, but constitute most of the available sites*. In Fig. 1a the isotherm is shown for $0.01 < C_x < 0.10$ mg/ml (or $100 > (1/C_x) > 10$ ml/mg), plotted as $1/w_{xs}$ *vs.* $1/C_x$ (which will linearize a Langmuir isotherm; *cf.* eqn. 2 of ref. 1). It is seen that this plot (based on calculated isotherm data) is indistinguishable from a Langmuir isotherm.

If a different range of mobile-phase concentrations is examined ($10 < C_x < 300$ mg/ml, or $0.1 > 1/C_x > 0.003$), as in Fig. 1b, the plot of $1/w_{xs}$ *vs.* $1/C_x$ is again linear, but with a different slope (the dashed curve in Fig. 1b corresponds to the solid curve in Fig. 1a). Note that the plot of Fig. 1a can be extrapolated to a value of $w_s \approx 1$ mg**, while the plot of Fig. 1b gives a value of $w_s \approx 100$ mg. That is, the plot of Fig. 1a is determined mainly by the lower-concentration, stronger sites ($w_s = 1$), while the plot of Fig. 1b reflects mainly the higher-concentration, weaker sites ($w_s = 100$). We will see that it is the stronger sites and smaller values of C_x that mainly determine chromatographic behavior during column overload.

Thus, within a certain range of solute concentration C_x, the system of Fig. 1 closely resembles a Langmuir isotherm. This has practical consequences for the effects of site heterogeneity on HPLC separations in the overload mode. In reversed-

---

* $w_{s1} = 1$ mg, $k_1 = 10$, $w_{s2} = 100$ mg, $k_2 = 1$, $V_m = 1$ ml.

** The y axis intercepts in Fig. 1 give the maximum column capacity ($1/w_s$); *e.g.*, $w_s = 1.2$ mg in Fig. 1a (*cf.* eqns. 3 and 4).

phase HPLC, silanol sites are usually present in small concentrations (for fully bonded packings), and their interaction with solute molecules can be much stronger than in the case of solvophobic interactions. In these cases, Langmuir retention may appear to be observed, as in Fig. 1a. However, the apparent column capacity w_s (extrapolated value from Fig. 1a), will then be much smaller than the maximum column capacity.

Localized adsorption. A detailed discussion of this phenomenon as it affects the adsorption isotherm is given in ref. 4 (where it is referred to as "restricted-access solvent delocalization"). While that discussion is specifically for the case of two-component mobile phases, the basic arguments are similar both for that case and for the case of solutions of a solute in a mobile phase (which are of interest here). When the adsorbent surface is covered with a high concentration of equivalent strong sites that occupy fixed positions on the adsorbent surface (*e.g.*, silanols on silica), and the adsorbate (solute) prefers to attach itself (localize) to these sites, all adsorbed solute molecules will be localized for lower coverages of the surface (values of θ_x). However, when θ_x exceeds about 0.7, the remaining surface is not favorable for localization, and further adsorption of solute will occur without localization. This means that the apparent retention (value of k' for delocalized molecules) will be much weaker than for localized solute molecules. The net effect is similar to that for a two-site surface (site heterogeneity as above). Thus, Langmuir plots ($1/w_{xs}$ *vs.* $1/C_x$) are found to be bimodal[3], just as in Fig. 1b for the case of a heterogeneous surface.

The theory developed[2–4] appears to give reliable predictions of the adsorption isotherm for cases involving both localizing and non-localizing solutes[4]. Elsewhere, we will explore its application to an understanding of the adsorption isotherm for silica and other polar adsorbents. Here, we are concerned mainly with overload separation in reversed-phase HPLC, and for these systems localized adsorption effects are generally unimportant. That is, reversed-phase packings do not normally have a high concentration of accessible strong sites (silanols). The Langmuir isotherm is actually a useful approximation for both cases, within a certain range of sample concentrations. This means that our model[1] for HPLC in the overload mode will be applicable over the same range of solute concentrations C_x.

A final comment can be made concerning site heterogeneity in reversed-phase HPLC *vs.* solute localization in normal-phase separations. In each case, the apparent value of w_s inferred from lower sample concentrations will be less than the maximum saturation capacity of the column. However, solute localization typically involves *ca.* 3/4 of the surface, so that the apparent w_s value at low values of C_x will then be *ca.* 3/4 of the maximum value. We will see in a following section that site heterogeneity in reversed-phase HPLC involves much smaller values of w_s for the low C_x part of the isotherm. Thus, the practical consequences (lower effective column loadability) are much more serious in the case of reversed-phase systems.

Non-unity stoichiometry of the sorption process

Extensive data, reviewed in refs. 2 and 4), show for adsorption chromatography with alumina or silica as column packing that large solute molecules displace more than one solvent molecule during retention of the solute. That is, eqn. 2 applies, n being determined by the molecular sizes of the solute X and mobile phase M molecules. Other studies[7,8] suggest that retention in reversed-phase HPLC is also governed

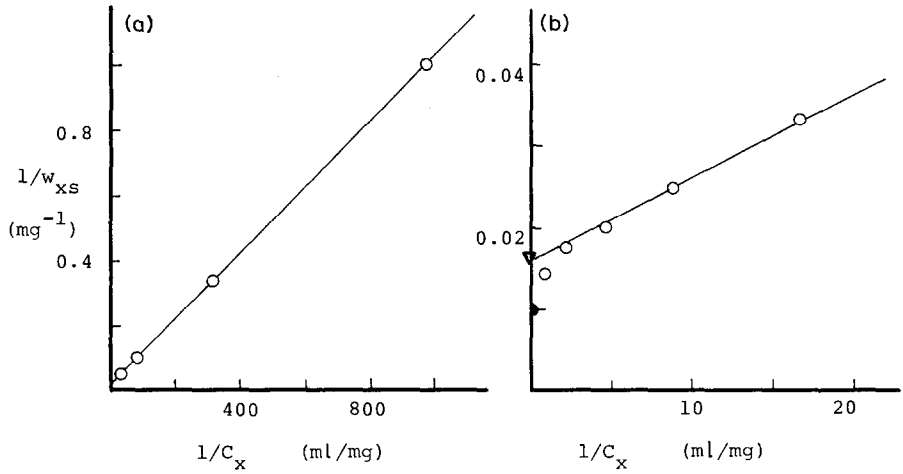

Fig. 2. Calculated isotherm for non-unity stoichiometry for a Langmuir-type isotherm (eqn. 2). Stoichiometry factor $n = 6$; $w_s = 100$ mg. See text for details. (a) Data for low values of C_x; (b) data for high values of C_x. ▽, ●, extrapolated values of $1/w_s$.

by a displacement process, so that eqn. 2 applies to these systems as well. For typical separations, values of n can vary widely[7,8].

The isotherm resulting from retention as described by eqn. 2 is derived in Appendix I. Fig. 2 shows a resulting isotherm for the case where $k_0 = 1$, stoichiometry factor $n = 6$, $w_s = 100$ mg and phase ratio $\varphi = 0.1$. Two different concentration ranges are plotted: $0.001 < C_x < 0.03$ in Fig. 2a, and $0.2 < C_x < 1$ mg/l in Fig. 2b. The solid line in Fig. 2b is an extension of the solid line from Fig. 2a, showing that the data appear to follow a Langmuir isotherm over almost the entire range of solute concentrations. The y-axis intercept (▽ in Fig. 2b) suggests a value of w_s equal to 67 mg, as compared to the maximum column capacity of 100 mg (● in Fig. 2b). We can conclude that systems with non-unity stoichiometry ($n \neq 1$) will not affect the application of our model[1] to the prediction of elution bands in the overload mode. However, apparent column capacities w_s will be lower than "true" values of w_s*.

Solute–solute interactions

As the concentration of solute in an HPLC system increases, interactions between solute molecules in both the mobile phase and stationary phase become more likely. In principle this might affect the thermodynamic activities of solute molecules in the two phases, resulting in deviations from Langmuir behavior. Other data[3] suggest that solute–solute and solvent–solute interactions frequently cancel in adsorption systems, for a variety of reasons. One exception to this would be the case of an ionized solute that does not exhibit ionic attraction to the stationary phase. An example is that of ionized carboxylic acids separated by reversed-phase chromato-

* A physical explanation for lower values of w_s when $n \neq 1$ is as follows. As the surface is progressively filled with adsorbed molecules of X, it becomes more difficult for an adsorbing molecule of X to locate two adjacent molecules of adsorbed M to replace.

graphy. As will be discussed later in this paper, these compounds appear to obey Langmuir sorption (eqn. 2 of ref. 1) but have much smaller (apparent) values of w_s, as a result of ionic repulsion between sorbed solute molecules.

Maximum column capacity w_s

First consider column packings with rigid surfaces, such as silica or alumina, and assume that the adsorbent surface is covered by a monolayer of solute (Langmuir adsorption). For this case, the maximum column capacity w_s can be estimated from the surface area (SA, m^2/g) of the column packing (see ref. 2 and Table III of ref. 3). The volume of the adsorbed monolayer per m^2 of surface is

$$\text{(silica)} \quad (V_s/\text{SA}) \approx 0.35\ \mu l/m^2 \tag{6}$$

and assuming a density of about 0.9 for the retained solute,

$$\text{(silica)} \quad (w_s/\text{SA}) \approx 0.3\ mg/m^2 \tag{7}$$

In the case of reversed-phase packings, the situation is more complex. First, the surface area of the starting silica is usually known, but this differs from the surface area of the resulting bonded-phase packing. In the case of small-pore silicas bonded with long alkyl groups (*e.g.*, C_{18}), a considerable reduction in apparent surface area can result (ref. 9 and Table VIII of ref. 10). We can estimate this surface-area reduction by assuming that (a) the bonded phase is equivalent to a liquid that coats the silica surface, thereby reducing the pore radius and the area of the surface of the bonded phase, and (b) all pores are cylinders of fixed diameter. Table I summarizes the resulting reduction in surface area as a function of the pore diameter of the silica and the chain length of the alkyl-bonded phase.

Another complication concerns the nature of the monolayer. In the case of inorganic adsorbents, it appears that molecules are generally adsorbed in a flat configuration, and this allows us to estimate the monolayer volume from eqn. 7. If some penetration of the bonded-phase surface occurs during reversed-phase retention (corresponding, to *e.g.*, vertical or "sideways" sorption, *cf.* ref. 11), we might expect values of w_s to be larger than those predicted by eqn. 7. Data from the present study provide further insight into this question.

TABLE I

EFFECTIVE SURFACE AREA (SA) OF BONDED-PHASE PACKINGS AS A FUNCTION OF PORE DIAMETER

Pore diameter (nm)	*Surface area of bonded-phase divided by surface area of silica*	
	C_8	C_{18}
6	0.80	0.55
8	0.86	0.69
10	0.89	0.76
15	0.93	0.85

EXPERIMENTAL

Chemical and reagents

Benzyl alcohol (>99% purity) was purchased from Aldrich (Milwaukee, WI, U.S.A.). Angiotensin II, human sequence, acetate salt (99% purity), insulin chain A, oxidized form from bovine insulin, caffeine, and 7β-hydroxypropyltheophyline were purchased from Sigma (St. Louis, MO, U.S.A.). Methanol and acetonitrile were HPLC grade, purchased from Fisher Scientific (Fair Lawn, NJ, U.S.A.). Water was purified and deionized with a Milli-Q water purification unit (Millipore, Bedford, MA, U.S.A.). Buffer salts were purchased from Fisher Scientific and from J. T. Baker (Phillipsburg, NJ, U.S.A.).

Columns

The isotherm measurements and the experimental loading studies were performed on Zorbax* ODS, C_8 and 150-C_8 5-μm and C_8 10-μm packing materials in either 5 cm × 4.6 mm I.D. or 15 cm × 4.6 mm I.D. columns.

Equipment

The instrumentation for the isotherm measurements and the experimental loading studies consisted of a Du Pont Model 8800 liquid chromatograph with a gradient controller, a Model 870 pump, a Model 864 variable-wavelength detector, a thermostatted column compartment and a Valco sampling valve Model CV-6UHPa-N60 (Du Pont, Wilmington, DE, U.S.A.). The analog data were digitized and stored by means of a Nelson analytical series interface (Nelson, Cupertino, CA, U.S.A.) and by means of a modified version of Nelson analytical chromatography software on an HP Series 220 microcomputer (Hewlett-Packard, Palo Alto, CA, U.S.A.). All polynomials were generated with the General Statistics Pac (Hewlett-Packard) and an HP-85 computer.

Procedures

Isotherm measurements. These measurements were performed by the breakthrough or frontal analysis method[12–14]. A relatively large volume, typically 1 or 2 ml of a mobile phase solution containing a known concentration of the solute was injected into the column. The volume of the injection was adjusted so that flat-topped peaks resulted. The concentration of the injected sample was varied over several orders of magnitude. The dead volume of the column was measured by an injection of concentrated sodium nitrate. In the case of angiotensin II as solute, it was observed that flat-topped peaks could be obtained only at lower flow-rates (which were used in these studies).

The uptake of solute by the stationary phase was calculated from the concentration of solute in the mobile phase plus the difference between the breakthrough volume and the dead volume of the column. The breakthrough volume was taken as the volume corresponding to the inflection point in the leading edge of the solute peak[14]. Table II summarizes these isotherm studies.

* Zorbax is Du Pont's registered trademark for its LC columns and packings.

TABLE II

SUMMARY OF ISOTHERM MEASUREMENTS

Column: 5 × 0.46 cm Zorbax C_{18}. See Figs. 3 and 4 and Experimental section for additional details. k_0 was calculated from the $V_m k_0$ value, assuming V_m = 0.47 ml.

Solute	*Mobile phase**	*Flow-rate (ml/min)*	w_s	$V_m k_0$	k_0
Benzyl alcohol	40% (v/v) M	0.9	67 ± 3	1.03 ± 0.01	2.2
	30% (v/v) M	0.9	63 ± 8	2.81 ± 0.01	6.0
		6.8	72 ± 20	2.80 ± 0.10	
	20% (v/v) M	0.9	62 ± 5	3.98 ± 0.06	8.5
Angiotensin II	15% (v/v) A	1.0	1**	5.9**	12.5
			60***	2.2***	4.7

* Mobile phase (see Experimental), M refers to concentration of methanol in water; A refers to acetonitrile concentration in aq. 0.1 *M* phosphate (pH 2.3).

** Values for adsorption onto strong sites (Fig. 4a).

*** Values for adsorption onto weak sites (Fig. 4b).

Chromatographic measurements. These measurements were performed by using small-volume injections (unless otherwise noted, sample volume = 15 μl) of various concentrations of a single solute, dissolved in the mobile phase. Values of k_0 and N_0 were calculated from injections of dilute solutions. Repeat measurements of k_0 and N_0 were performed periodically throughout each study; this allowed correction for any changes in column performance (values of k_0 and N_0).

The retention volume V_R ("cumulative" value in ref. 1) of each peak was determined as the volume at which 50% of the sample was eluted. Values of bandwidth σ_v were calculated as 1/2 the difference between the volumes at which 15.9% and 84.1% of the sample was eluted from the column.

The detection wavelength was chosen so that an absorbance value of 1.0 was not exceeded; however, Beer's law non-linearities were still observed in the benzyl alcohol studies. For this case, calibration curves were obtained from the steady-state absorbance values for large-volume injections of known solute concentrations. Calibration curves fit by a polynomial were used to correct for non-linearity within short intervals across the solute elution band. Values of V_R (and k') and σ_v (and N) were calculated from the resulting (corrected for non-linearity) cumulative elution band, as described above.

Chromatographic data with small sample sizes are given in Table III, while a complete tabulation of individual data points for both isotherm measurements and loading studies is given in ref. 15.

RESULTS AND DISCUSSION

Isotherm measurements

Isotherms were measured experimentally for a 5-cm reversed-phase column (Zorbax ODS, a 6-nm-pore C_{18} packing) and two solutes: benzyl alcohol and angiotensin II. Three different mobile phase compositions were used for benzyl alcohol.

TABLE III

SUMMARY OF EXPERIMENTAL HPLC RUNS UNDER OVERLOAD CONDITIONS
Columns used are 5 × 0.46 cm, except for caffeine and 7β-hydroxypropyltheophyline (15 × 0.46 cm).

Solute	*Column*	*Mobile phase**	*Flow-rate (ml/min)*	k_0**	N_0**	A_s
Benzyl alcohol	ODS	20% M	0.9	7.6	2280	1.1
			6.8	11.2	1440	1.2
		30% M	0.9	5.8	3060	1.1
			6.8	5.8	1100	1.2
		40% M	0.9	2.9	1810	1.2
			6.8	3.5	990	1.2
	C_8	30% M	1.0	5.9	3550	1.0
	150-C_8	30% M	1.0	3.3	2900	1.1
Angiotensin II	ODS	15% A in B	1.0	12.8	1880	1.3
	C_8	18% A in B	0.5	4.1	485	2.4
	150-C_8	18% A in B	0.5	9.7	1690	1.7
Insulin A chain	C_8	17% A in B′	0.4	9.0	550	1.6
Caffeine	C_8	5% A, 20% M in B″	1.0	2.9	5600	1.5
7β-Hydroxypropyl-theophyline	C_8	5% A, 20% M in B″	1.0	2.6	6500	1.1

* Percentages refer to % (v/v) organic in water or buffer mobile phase; M refers to methanol, A refers to acetonitrile, B refers to 0.1 *M* phosphate buffer (pH 2.3), B′ refers to 0.1 *M* phosphoric acid plus triethylamine (pH 2.2), and B″ refers to 0.1 *M* monobasic sodium phosphate.

** Different columns were used, resulting in some variation in k_0 and N_0.

The procedure followed is described in the Experimental section; it consisted of measurements on the same (or a similar) column later used for HPLC studies, as a function of sample size and experimental conditions (following section).

Benzyl alcohol. Results for benzyl alcohol and methanol–water (40:60) are shown in Fig. 3. In Fig. 3a the data points cover the range $0.2 < C_x < 20$ mg/ml, and the resulting plot is seen to be linear within experimental error (Langmuir behavior). Fig. 3b shows a similar plot, covering the range $40 < C_x < 200$ mg/ml, with the solid curve from Fig. 3a superimposed onto that in Fig. 3b. This system appears to exhibit Langmuir behavior over the entire range of concentrations studied ($0.2 < C_x < 200$ mg/ml). Pair-wise calculations (values of w_s *vs.* C_x) yield values of both the intercept ($1/w_{xs}$) and slope ($1/V_m k_0$) for this system, as summarized in Table II*.

Similar measurements were performed by using mobile phases of varying composition (20–40% (v/v) methanol in water), as well as at different flow-rates. The

* Note that fitting the data in Fig. 3 on a single plot with a least-squares line is insensitive to isotherm non-linearity, as in Fig. 1. The reason is that deviant data points at large values of C_x show negligible deviations in $1/w_{xs}$; correlation coefficients are therefore close to 1, even for plots as in Fig. 1 and 2. For this reason we have presented all isotherm data in the form of complementary plots (Figs. 1–4).

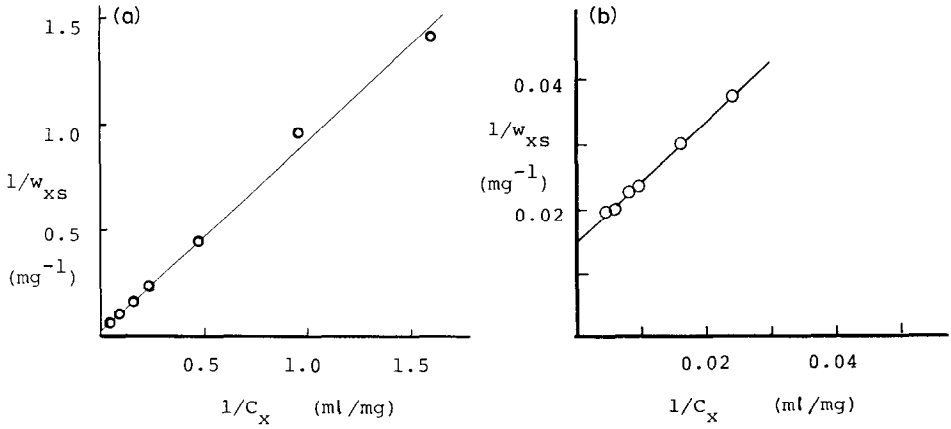

Fig. 3. Experimental isotherm data for benzyl alcohol as solute. Mobile phase, methanol–water (40:60); column, 5 × 0.46 cm Zorbax ODS. (a) Data for low solute concentrations, $0.2 \leqslant C_x \leqslant 20$ mg/ml; (b) data for high solute concentrations, $40 \leqslant C_x \leqslant 200$ mg/ml.

resulting isotherm plots resembled those of Fig. 3, showing Langmuir-isotherm behavior over wide ranges in C_x: methanol–water (30:70), $0.1 < C_x < 30$ mg/ml; methanol–water (20:80), $0.1 < C_x < 40$ mg/ml. Resulting values of w_s from these different isotherm measurements are summarized in Table II, and are seen to be constant within experimental error: 64 ± 6 (1 S.D.) mg for a flow-rate of 0.9 ml/min. These results, together with the Langmuir plots as in Fig. 3, confirm that this system follows Langmuir behavior; *i.e.*, true Langmuir adsorption must yield a constant value of w_s for a given solute/column combination.

Angiotensin II. Fig. 4 presents Langmuir plots for angiotensin II as solute and the same column as for benzyl alcohol. Fig. 4a shows the isotherm for the concentration range $0.07 < C_x < 0.35$ mg/ml, with good adherence of the data to a linear plot (apparent Langmuir behavior). However, the extrapolated value of w_s is quite small (only 2 mg). This suggests site heterogeneity, and this is confirmed by isotherm measurements at higher values of C_x: $0.3 < C_x < 7$ mg/ml, as summarized in Fig. 4b. The dashed curve in Fig. 4b is taken from Fig. 4a, and the data for large C_x are seen to deviate markedly from that curve. The latter points can be extrapolated to a value of $w_s \approx 60$ mg, which is much larger than for the case of Fig. 4a, but close to the result for benzyl alcohol ($w_s = 64$) in Fig. 3.

We can use adjacent points in the plots of Figs. 4a and b to solve eqn. 2 of ref. 1 for values of w_s and $V_m k_o$, as a function of the total uptake of angiotensin II by the column (w_{xs}). Resulting values of the apparent column capacity w_s are plotted against w_{xs} in Fig. 4c. It is seen that these change regularly as w_{xs} increases, tending to a value of about 1 mg at low value of w_{xs}, and tending to a value of about 60 mg at high values of w_{xs}. The dashed line at $w_s = 64$ mg in Fig. 4c corresponds to the expected value from the benzyl alcohol data, assuming that the maximum uptake of either solute by the column will be the same (as expected, approximately, for a simple Langmuir system; eqn. 7).

These observations suggest that two types of sites contribute to the retention of angiotensin II in this system. Presumably residual silanols comprise the strong

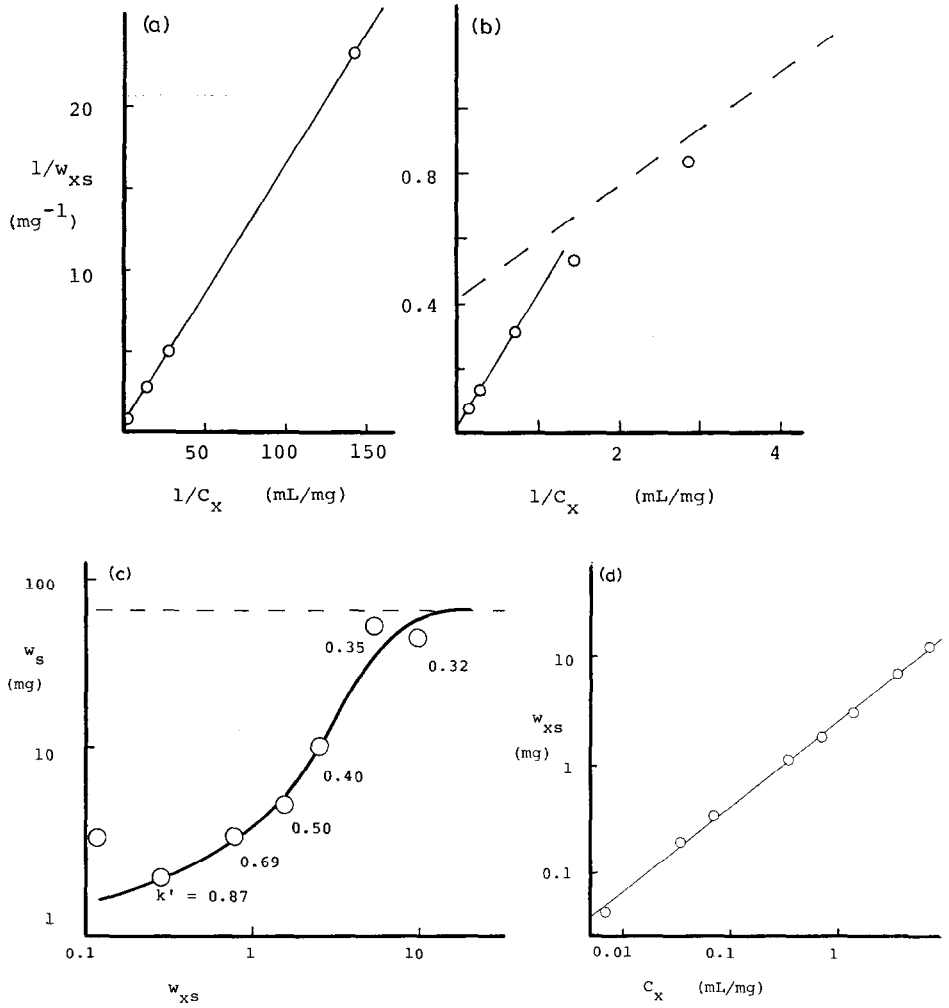

Fig. 4. Experimental isotherm data for angiotensin II as solute. Mobile phase, acetonitrile–0.1 *M* aqueous phosphate (pH 2.3) (15:85); column, 5 × 0.46 cm Zorbax ODS. (a) Data for low solute concentrations, $0.07 \leqslant C_x \leqslant 0.35$ mg/ml; (b) data for high solute concentrations, $0.3 \leqslant C_x \leqslant 7$ mg/ml; (c) apparent w_s values *vs.* weight of solute in stationary phase (w_{xs}); (d) log w_{xs} *vs.* log C_x plot (Freundlich isotherm plot).

sites, and constitute about 2% of the available surface of the packing. Values of k_0, derived from these data and summarized in Table I, suggest that the strong sites have a k_0-value about 3-times greater than for the weak sites (small sample sizes). Together with the site–concentration ratio ($\approx 1/60$ for silanols), this suggests that the equilibrium distribution constant K for the silanols is about 200 times larger than for binding of angiotensin II to the hydrophobic surface.

It should be noted that the isotherm data of Fig. 4a and b can be described by the Freundlich isotherm[4]:

$$w_{xs} = g\, C_x^h \tag{8}$$

Here, g and h are constants for a given system. Eqn. 8 predicts linear plots of log w_{xs} *vs.* log C_x, and this is observed for the angiotensin II data in Fig. 4d. The Freundlich isotherm is a purely empirical fitting function, so that the correlation of Fig. 4d has no fundamental significance. However, it should be noted that the Freundlich isotherm is often a good approximation for isotherms that are non-Langmuir (as in this case, for a wide range of C_x values). Later, we will see that our model in ref. 1 (which assumes Langmuir behavior) fits the angiotensin II system rather well. This suggests its similar utility for other non-Langmuir-isotherm systems that follow the Freundlich isotherm.

Chromatographic data under overload conditions

Single-solute samples were chromatographed under the same conditions (and on the same columns) as those used for the isotherm studies. This alowed a direct correlation of experimental values of k', N and band shape with values predicted by the model in ref. 1. Additional chromatographic data were obtained for other solutes and experimental conditions (different column types), but without measuring isotherms. These runs allow a further check of experimental data against the model.

Table III summarizes the various HPLC systems studied in an overload chromatographic mode. Values of k_0 and N_0 are given for each series of runs, as well as band asymmetry A_s for small sample injections. Data for the various runs at higher sample size are summarized in the following figures and tables. A complete tabulation of these results can be obtained from ref. 15.

The model presented in ref. 1 predicts that experimental values of k'/k_0 and N/N_0 should be correlated with values of the loading functions w_{xk} and w_{xN}, respectively. These functional dependencies were defined from Craig simulations, as summarized in Table II of ref. 1. These "master curves" are shown in Fig. 5a–c as dashed lines. Fig. 5a and b are for "cumulative" values of k' and N; we will be

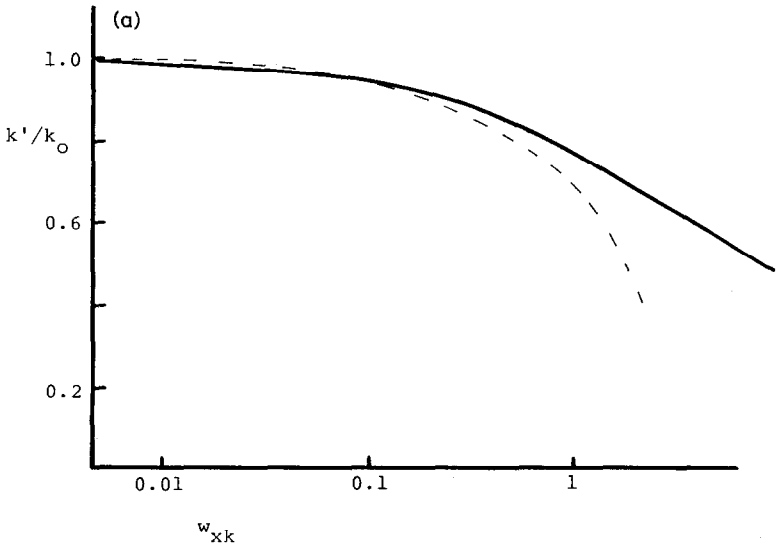

Fig. 5.

(*continued on p. 58*)

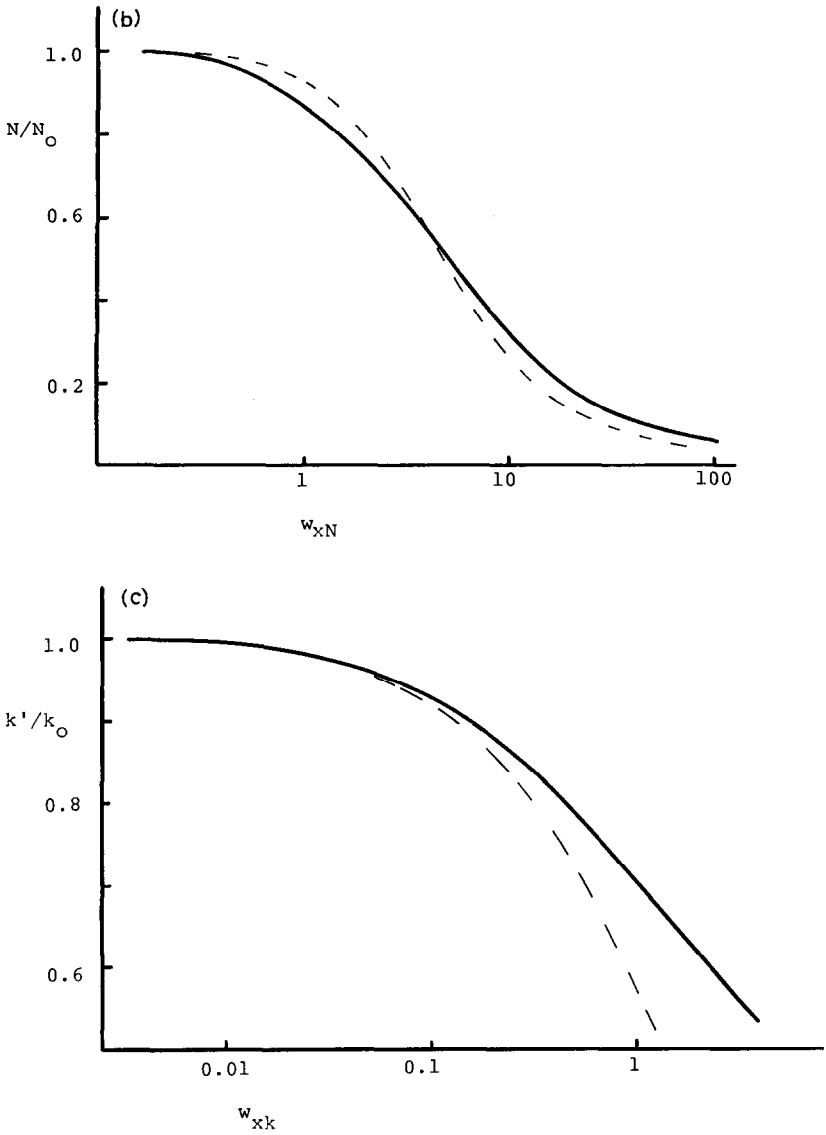

Fig. 5. Dependence of k'/k_0 and N/N_0 on w_{xk} and w_{xn}, respectively. (a) "Cumulative" values of k'; (b) "cumulative" values of N; (c) "band" values of k'. (– – –) Craig-model values from Table II of ref. 1; (———) empirical, best-fit values from present study.

concerned with these correlations for the most part. When experimental values of k'/k_0 and N/N_0 were compared with Fig. 5a and b, it was found that an approximate superimposition of experimental data and master curves could be obtained. However, a slight adjustment in the shape of the master curves (solid curves in Fig. 5a and b) was found to give a better overall fit to the experimental data. Presumably, this reflects subtle differences between the Craig model and "real" HPLC separations.

TABLE IV

EMPIRICAL BEST-FIT DEPENDENCE OF k'/k_0 AND N/N_0 *vs.* THE LOADING FUNCTIONS w_{xk} AND w_{xN} (FIG. 5)

Cumulative values of k'/k_0 *vs.* w_{xk} and N/N_0 *vs.* w_{xN} can also be expressed mathematically. Appropriate fitting functions are available from the authors.

w_{xk} *or* w_{xN}	k'/k_0	N/N_0	w_{xk} *or* w_{xN}	k'/k_0	N/N_0
*"Cumulative" values (Fig. 5a,b)**					
0.01	0.99	1.00	2	0.69	0.74
0.02	0.98	1.00	5	0.57	0.51
0.05	0.97	1.00	10	0.48	0.32
0.10	0.95	1.00	20	(0.39)	0.19
0.20	0.92	1.00	50	(0.27)	0.10
0.50	0.85	0.95	100	(0.18)	0.06
1.00	0.77	0.87	200		0.04
w_{xk}	(k'/k_0)	w_{xk}	(k'/k_0)		
*"Band" values (Fig. 5c)***					
0.01	0.99	0.5	0.79		
0.02	0.98	1	0.71		
0.05	0.96	2	0.62		
0.10	0.93	5	0.50		
0.20	0.88	10	0.41		

* As in Fig. 1b of ref. 1.
** As in Fig. 1a of ref. 1.

We therefore used the solid curves in Fig. 5a and b in further correlations of experimental data. These latter loading function curves are listed in Table IV.

Benzyl alcohol, Zorbax ODS column. Sample sizes of 0.003–5 mg were injected, the data for the elution band were expressed as cumulative percent *vs.* time curves (*e.g.*, as in Fig. 1b of ref. 1), and values of k' and N ("cumulative" values) were obtained. The loading functions w_{xk} and w_{xN} were then calculated for each sample mass, and values of k'/k_0 were plotted against w_{xk} w_s (Fig. 6). Similarly, N/N_0 was plotted against w_{xN} w_s in Fig. 7*. For a particular solute and column (where w_s is constant), the resulting data should describe a plot that can be superimposed onto one of the master curves of Fig. 5a and b. This is seen to be the case for both Figs. 6 and 7.

The best curve through the data of Figs. 6 or 7 corresponds to some value of w_s in each case. This w_s value is obtained by simply overlaying plots as in Figs. 6 and 7, onto the corresponding curves from Fig. 5a or b. The value of the x axis from the experimental-data plots that corresponds to $x = 1$ from the plots of Fig. 5 then equals the best-fit value of w_s. For the k' data of Fig. 6, the best-fit value of w_s is found to be about 90 mg. Similarly, the best-fit value of w_s for the data of Fig. 7 is 30 mg. Note that the isotherm value of 64 mg lies midway between these two values (30 and 90 mg). At this point, we see that the predicted curves for k' and N as a

* At this point, we assume that w_s is not known; w_{xk} w_s is then equal to $[k_0/(1+k_0)]$ $N_0^{0.5}$ w_x, and w_{xN} w_s $= [k_0/(k_0+1)]^2$ $N_0 w_x$.

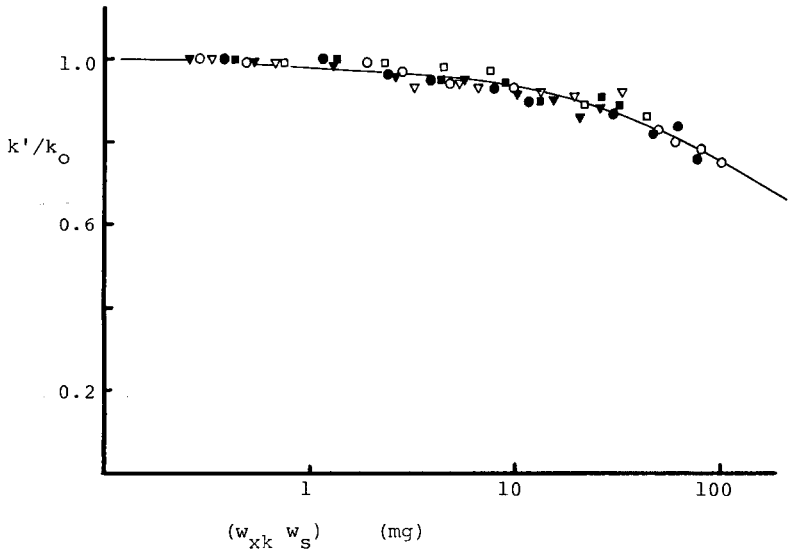

Fig. 6. Chromatographic data for benzyl alcohol and Zorbax ODS column: dependence of k'/k_0 on w_{xk} w_s. (———) Superimposed master curve of Fig. 5a, best-fit value of w_s = 90 mg. Experimental data points:

Methanol–water (v/v)	0.89 ml/min	6.8 ml/nmin
20:80	▽	▼
30:70	□	■
40:60	○	●

Other conditions described in Experimental section.

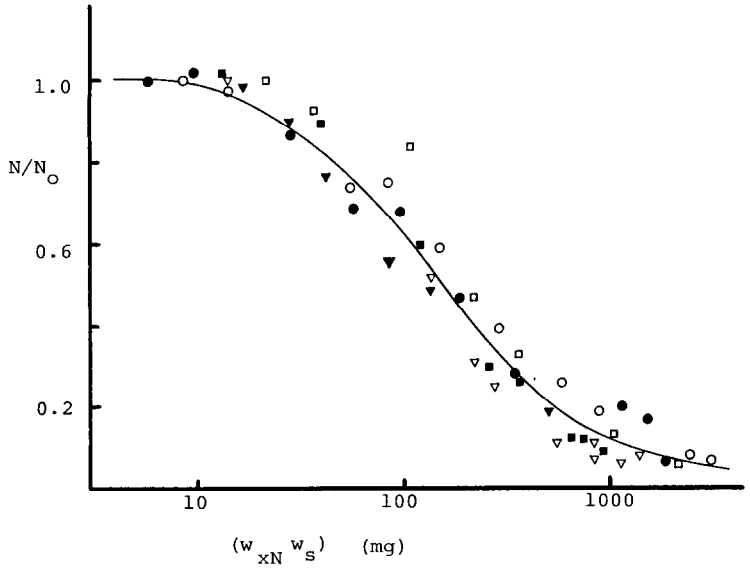

Fig. 7. Chromatographic data for benzyl alcohol and Zorbax ODS column: dependence of N/N_0 on $w_{xN}w_s$. (———) Superimposed master curve of Fig. 5b, best-fit value of w_s = 30 mg. Symbols for data points as in Fig. 5.

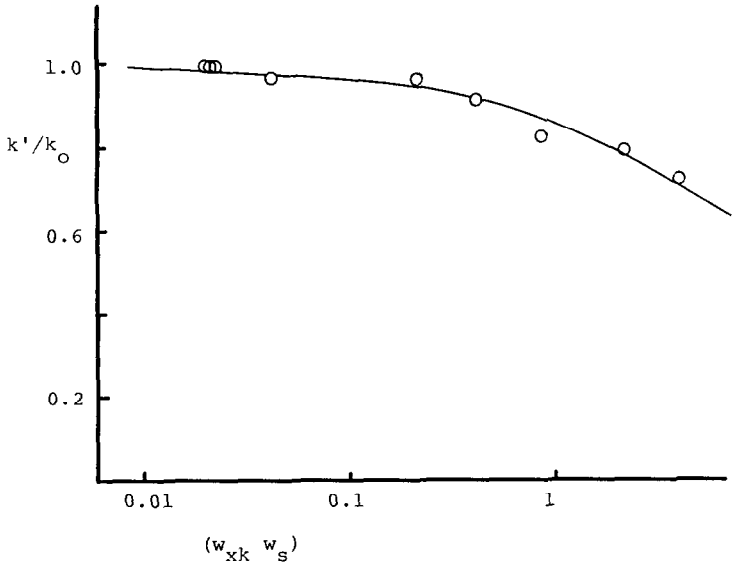

Fig. 8. Chromtographic data for angiotensin II and Zorbax ODS column: dependence of k'/k_0 on w_{xk} w_s. Mobile phase, acetonitrile–0.1 *M* phosphate (pH 2.3) (15:85); flow-rate, 1 ml/min. (———) Superimposed master curve of Fig. 5a, best-fit value of w_s = 2.5 mg. (○) Experimental data points. Other conditions in Experimental section.

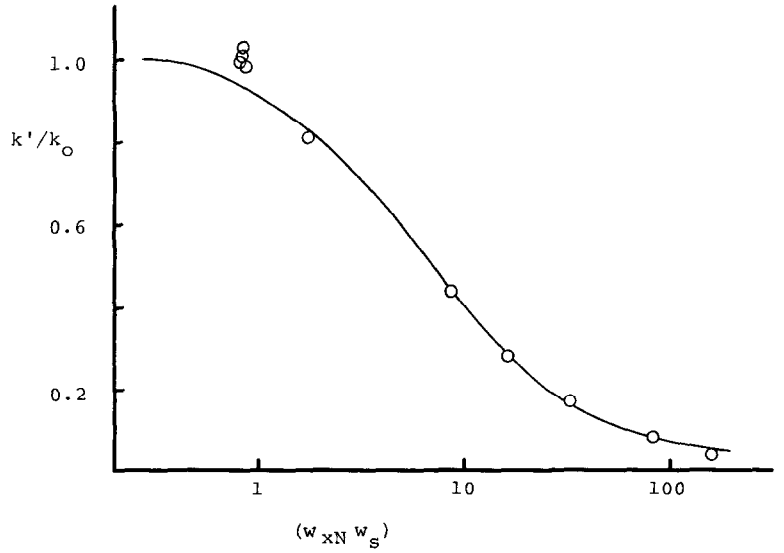

Fig. 9. Chromatographic data for angiotensin II and Zorbax ODS column: dependence of N/N_0 on w_{xk} w_s. Conditions as in Fig. 8. (———) Superimposed master curve of Fig. 5b, best-fit value of w_s = 1.4 mg; (○) Experimental data points.

function of sample size (using the isotherm value of 64 mg) give an approximate prediction of the two experimental curves of Figs. 6 and 7. We will discuss these different values of w_s, obtained from k'/k_0 *vs.* N/N_0 plots, later, after reviewing additional data for other solutes and columns (however at the present time we do not have an explanation for this effect).

Angiotensin II, Zorbax ODS column. Sample sizes of 0.5–105 μg angiotensin II were injected in this series of runs, and the same conditions were used as for the isotherm studies of Fig. 4 and Table II. The results are plotted in Figs. 8 and 9 in the same way as for benzyl alcohol in Figs. 6 and 7. Again, a reasonable adherence of the experimental values of k'/k_0 and N/N_0 to the predicted curves (Fig. 5) is seen. The best-fit values of w_s are 2.5 mg for the k'/k_0 data, and 1.4 mg for the N/N_0 data. These values are in rough agreement with the small-sample w_s value from the isotherm measurements (1 mg), suggesting that the strong sites largely determine the effective value of w_s — as far as values of k'/k_0 and N/N_0 are concerned. Reference to Fig. 4d is also helpful in this connection. From Fig. 8. we see that the average value of k'/k_0 is about 0.85, for values of k'/k_0 significantly different from unity. Fig. 4d suggests a value of w_s for this average sample size (or value of w_{xs}) equal to about 2 mg (a value that is midway between the above values of 1.4 and 2.5 mg, from chromatographic runs). These comparisons are summarized in Table II.

The following discussion emphasizes values of w_s obtained as in the preceding example, for other HPLC systems. We will see that values of w_s vary with both the solute and the column, and that larger values of w_s are consistently observed for plots of k'/k_0 as compared with plots of N/N_0. Later we will show that values of w_s for predicting values of k'/k_0 and N/N_0 —and therefore the elution curve as a function of sample loading— can be obtained from a few experiments under overload con-

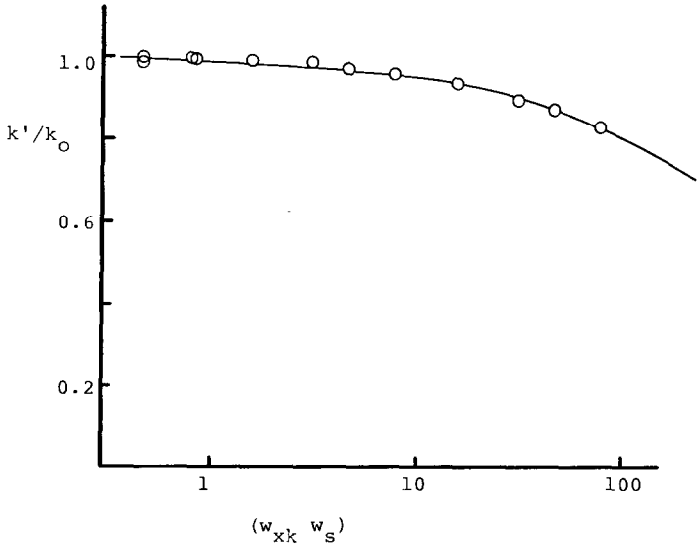

Fig. 10. Chromatographic data for benzyl alcohol and Zorbax C_8 column: dependence of k'/k_0 on w_{xk} w_s. Mobile phase methanol–water (30:70); flow-rate, 1 ml/min. (———) Superimposed master curve of Fig. 5a, best-fit value of w_s = 140 mg. (○) Experimental data points.

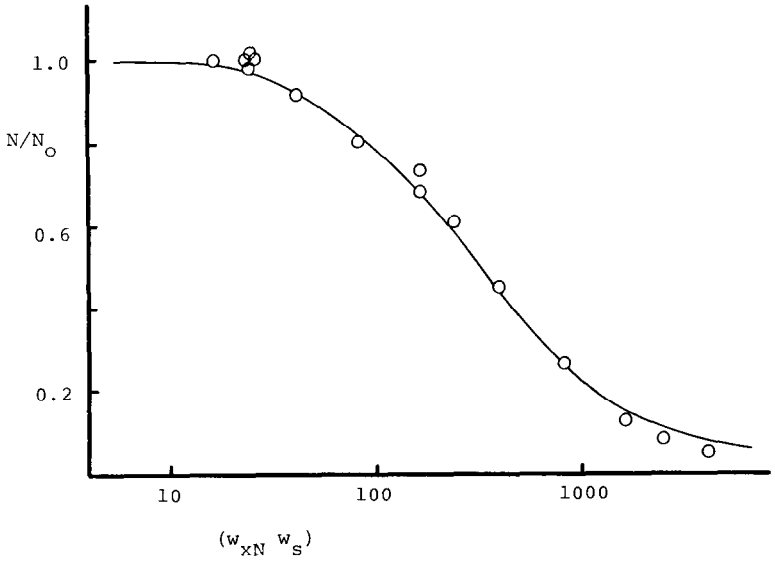

Fig. 11. Chromatographic data for benzyl alcohol and Zorbax C_8 column: dependence of N/N_0 on w_{xN} w_s. Conditions as in Fig. 10. (———) Superimposed master curve of Fig. 5b, best-fit value of w_s = 60 mg. (○) Experimental data points.

ditions. This allows the easy application of the present approach (model simulations) to actual HPLC separation in an overload mode.

Other overload HPLC studies

Several other systems were investigated, involving different solutes and col-

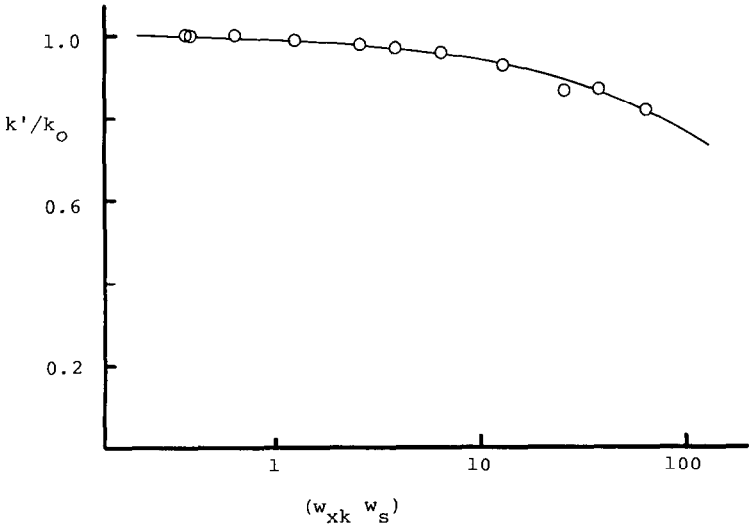

Fig. 12. Chromatographic data for benzyl alcohol and Zorbax 150-C_8 column: dependence of k'/k_0 on w_{xk} w_s. Mobile phase, methanol–water (30:70); flow-rate, 1 ml/min. (——). Superimposed master curve of Fig. 5a, best-fit value of w_s = 100 mg. (○) Experimental data points.

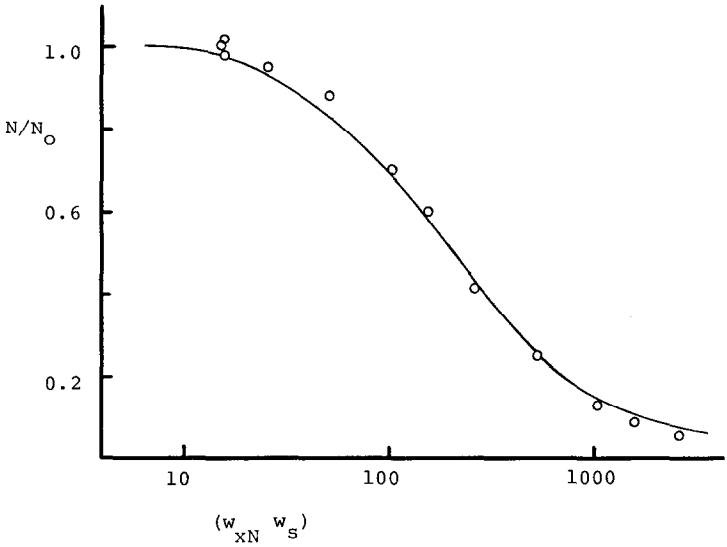

Fig. 13. Chromatographic data for benzyl alcohol and Zorbax 150-C_8 column: dependence of k'/k_0 on w_{xk} w_s. Conditions as in Fig. 12. (———) Superimposed master curve of Fig. 5b, best-fit value of w_s = 40 mg. (○) Experimental data points.

umns. These data are summarized in Figs. 10–23 and Table V. The correlations of Figs. 10–23 with the (solid) master curves of Fig. 5a and b are seen to be generally satisfactory. The best-fit values of w_s for these various correlations are summarized in Table V, although isotherm data for comparison were not collected. In the resulting data of Table V, certain general trends are apparent, which we will examine.

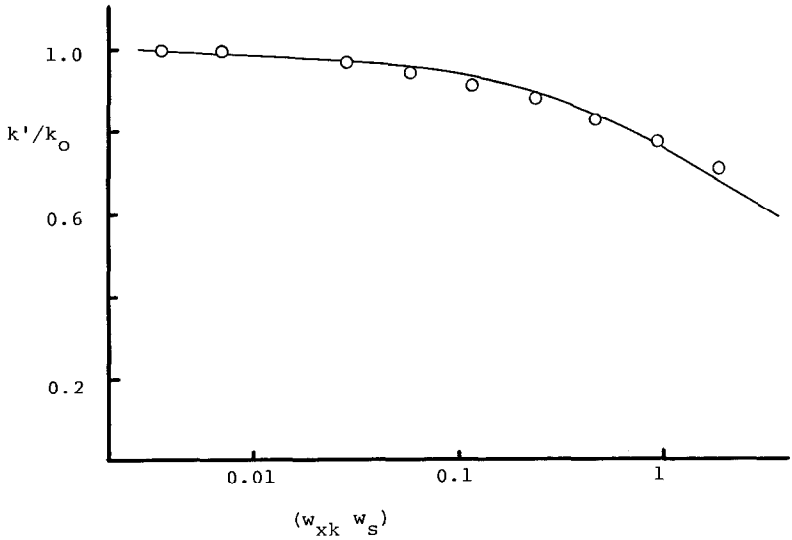

Fig. 14. Chromatographic data for angiotensin II and Zorbax C_8 column: dependence of k'/k_0 on w_{xk} w_s. Mobile phase, acetonitrile–0.1 *M* phosphate buffer (pH = 2.3) (18:72); flow-rate, 0.5 ml/min. (———) Superimposed master curve of Fig. 5a, best-fit value of w_s = 0.9 mg. (○) Experimental data points.

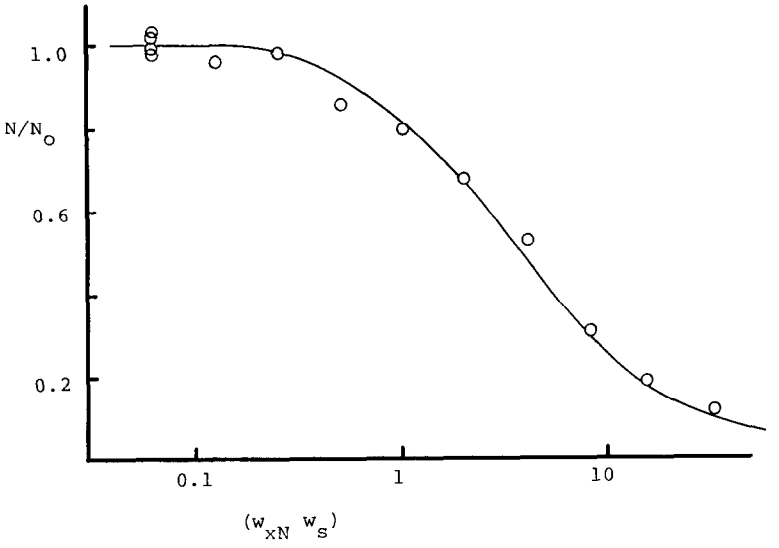

Fig. 15. Chromatographic data for angiotensin II and Zorbax C_8 column: dependence of N/N_0 on w_{xN} w_s. Conditions as in Fig. 14. (———) Superimposed master curve of Fig. 5b, best-fit value of w_s = 0.7 mg. (O) Experimental data points.

Effects of flow-rate and mobile phase composition on overload separation. The plots of Figs. 6 and 7 for benzyl alcohol and the ODS column show more scatter than later plots for other solute–column combinations. The data of Figs. 6 and 7 include runs where flow-rate (and N_0) and mobile phase composition (and k_0) were

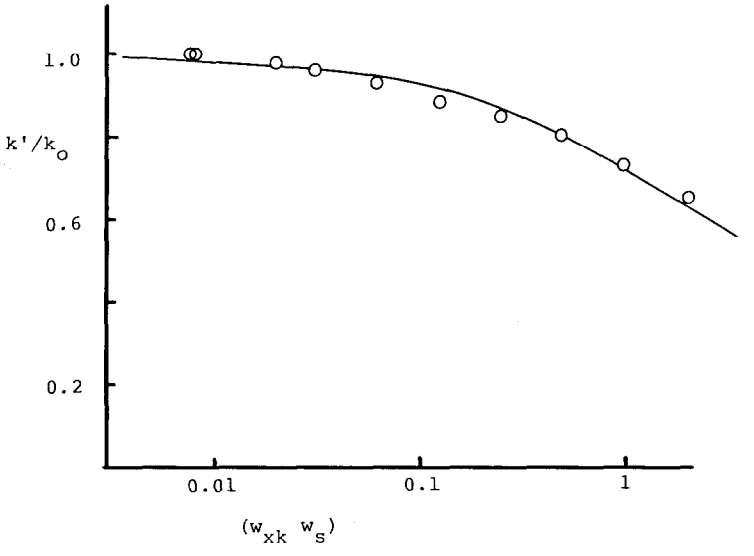

Fig. 16. Chromatographic data for angiotensin II and Zorbax 150-C_8 column: dependence of k'/k_0 on w_{xk} w_s. Mobile phase, acetonitrile–0.1 *M* phosphate buffer (pH = 2.3) (18:82); flow-rate, 0.5 ml/min. (———) Superimposed master curve of Fig. 5a, best-fit value of w_s = 0.7 mg. (O) Experimental data points.

TABLE V

COMPARISON OF VALUES OF COLUMN CAPACITY w_s OBTAINED FROM ISOTHERM AND CHROMATOGRAPHIC MEASUREMENTS

Solute	*Column*	w_s *(mg)*			
		Isotherm	*HPLC*		
			k'/k_0	N/N_0	*Ratio**
Benzyl alcohol	Zorbax ODS	64	90	30	3.0
	Zorbax C_8		140	60	2.3
	Zorbax 150-C_8		100	40	2.5
Angiotensin II	Zorbax ODS	2**	2.5	1.4	1.8
	Zorbax C_8		0.9	0.7	1.3
	Zorbax 150-C_8		0.7	0.55	1.4
Insulin A chain	Zorbax C_8		1.3	0.5	2.3
Caffeine	Zorbax C_8		180	50	3.6
7β-Hydroxypropyl-theophyline	Zorbax C_8		300	70	4.5
				Average	2.5 ± 1.0

* Ratio of w_s value from k'/k_0 *vs.* w_s value from N/N_0.
** Value from Fig. 4d (see text).

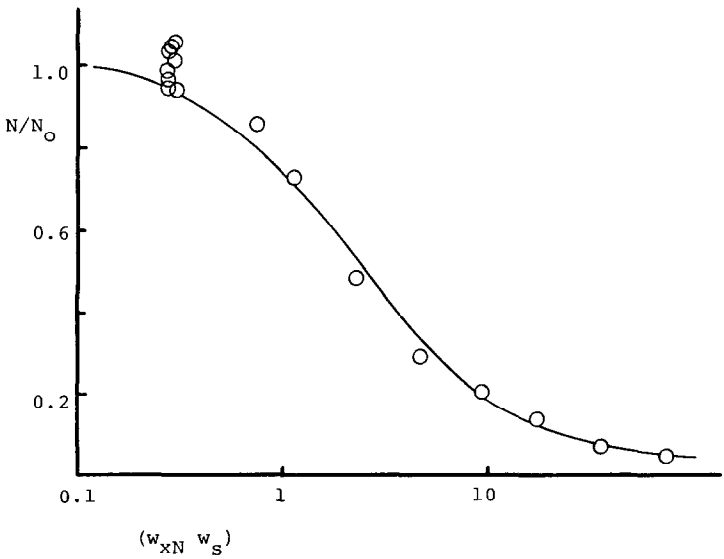

Fig. 17. Chromatographic data for angiotensin II and Zorbax 150-C_8 column: dependence of N/N_0 on w_{xN} w_s. Conditions as in Fig. 16. (———) Superimposed master curve of Fig. 5b, best-fit value of w_s = 0.5 mg. (○) Experimental data points.

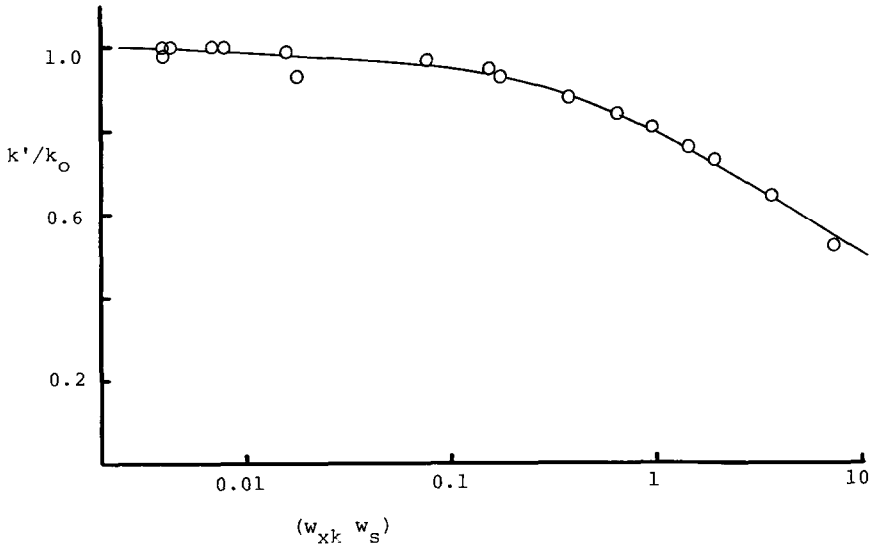

Fig. 18. Chromatographic data for insulin A chain and Zorbax ODS column: dependence of k'/k_0 on w_{xk} w_s. Mobile phase, acetonitrile–0.1 *M* phosphate (pH = 2.3) (27:73); flow-rate, 0.4 ml/min. (———) Superimposed master curve of Fig. 5a, best-fit value of w_s = 1.3 mg. (○) Experimental data points.

varied; in later studies (Figs. 8–23) the flow-rate or the mobile phase was not varied. It is therefore possible that the greater scatter in Figs. 6 and 7 reflects systematic effects due to N_0 and k_0 that have not been adequately corrected for. To answer this question, the runs in Figs. 6 and 7 were segregated according to flow-rate and solvent composition, and were replotted (Fig. 24).

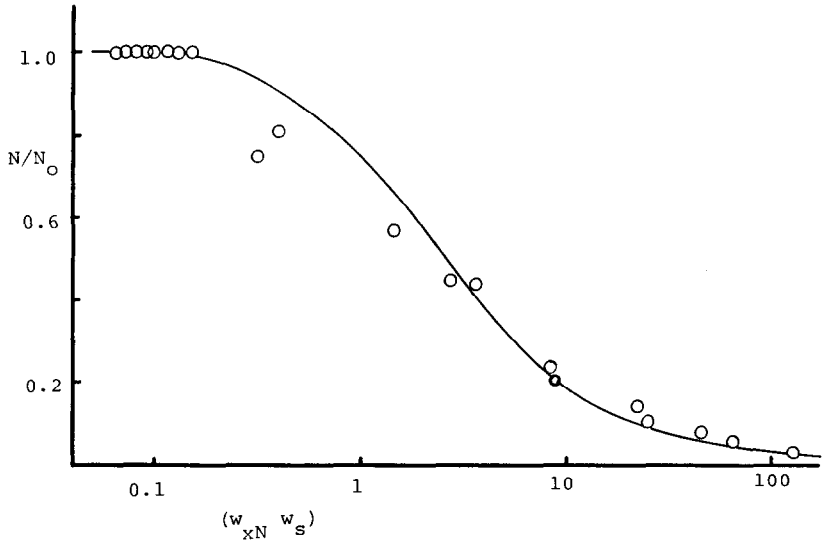

Fig. 19. Chromatographic data for insulin A chain and Zorbax ODS column: dependence of N/N_0 on w_{xN} w_s. Conditions as in Fig. 18. (———) Superimposed master curve of Fig. 5b, best-fit value of w_s = 0.5 mg. (○) Experimental data points.

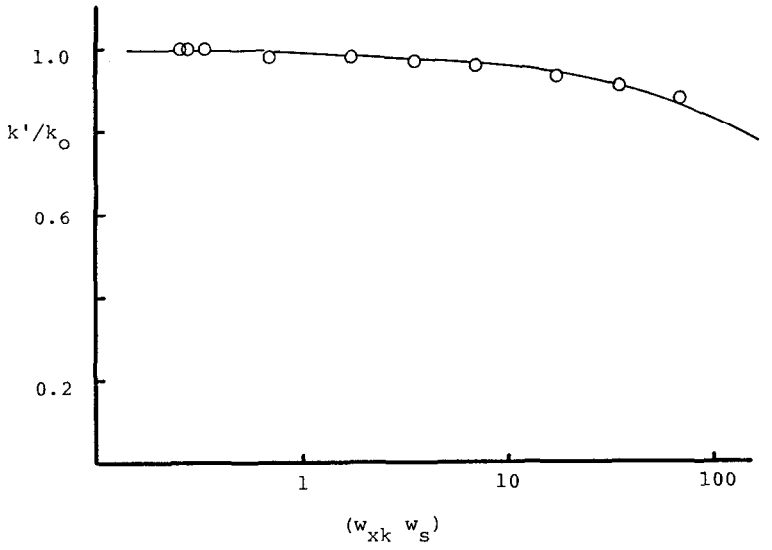

Fig. 20. Chromatographic data for caffeine and 15-cm Zorbax C_8 column: dependence of k'/k_0 on w_{xk} w_s. Mobile phase, methanol–acetonitrile–0.01 *M* phosphate buffer (pH = 4.0) (20:5:75); flow-rate, 1 ml/min. (———) Superimposed master curve of Fig. 5a, best-fit value of w_s = 180 mg. (○) Experimental data points.

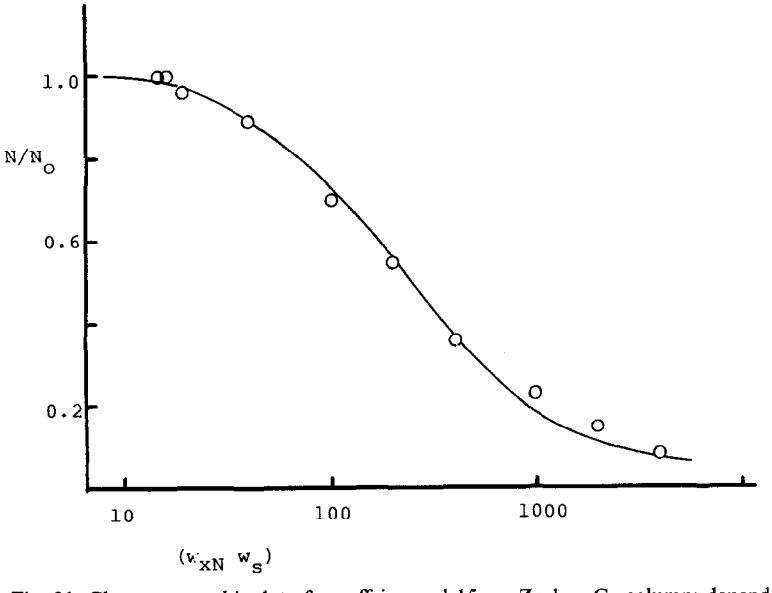

Fig. 21. Chromatographic data for caffeine and 15-cm Zorbax C_8 column: dependence of N/N_0 on w_{xN} w_s. Conditions as in Fig. 20. (———) Superimposed master curve of Fig. 5b, best-fit value of w_s = 50 mg. (○) Experimental data points..

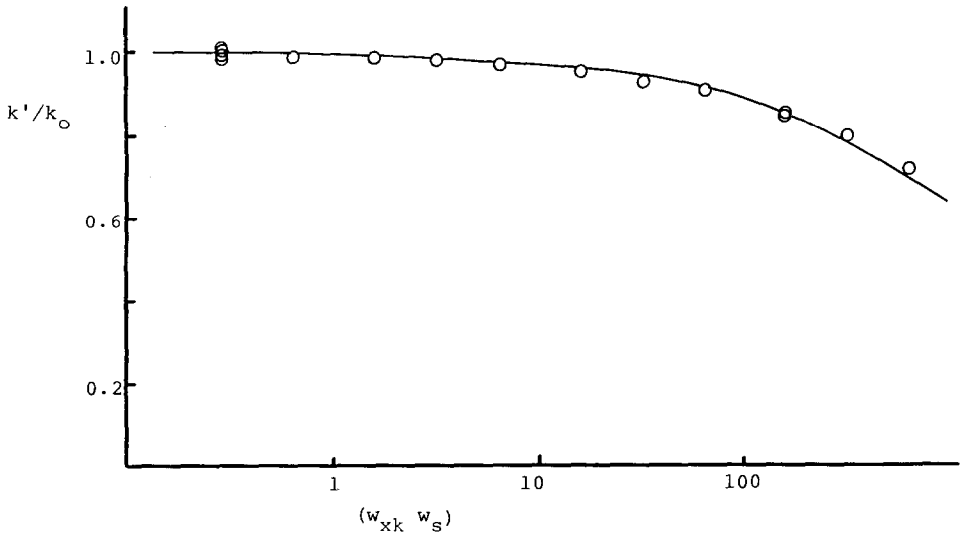

Fig. 22. Chromatographic data for 7β-hydroxypropyltheophyline and 15-cm Zorbax C_8 column: dependence of k'/k_0 on w_{xk} w_s. Conditions as in Fig. 20. (— —) Superimposed master curve of Fig. 5a, best-fit value of w_s = 300 mg. (O) Experimental data points.

Fig. 24 shows that the experimental scatter in these plots is reduced (*cf.* Figs. 6 and 7), suggesting additional (unrecognized) contributions from flow-rate or mobile phase composition. Values of w_s were derived for each of the plots of Fig. 24 and are summarized in Table VI.

Our conclusion is that values of the effective column capacity w_s vary in minor

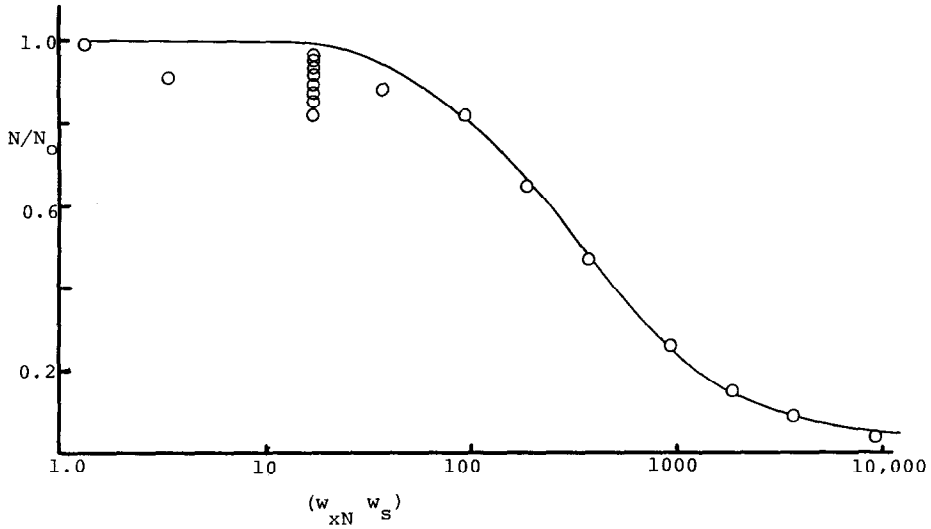

Fig. 23. Chromatographic data for 7β-hydroxypropyltheophyline and 15-cm Zorbax C_8 column: dependence of N/N_0 on w_{xN} w_s. Conditions as in Fig. 20. (———) Superimposed master curve of Fig. 5b, best-fit value of w_s = 70 mg. (O) Experimental data points.

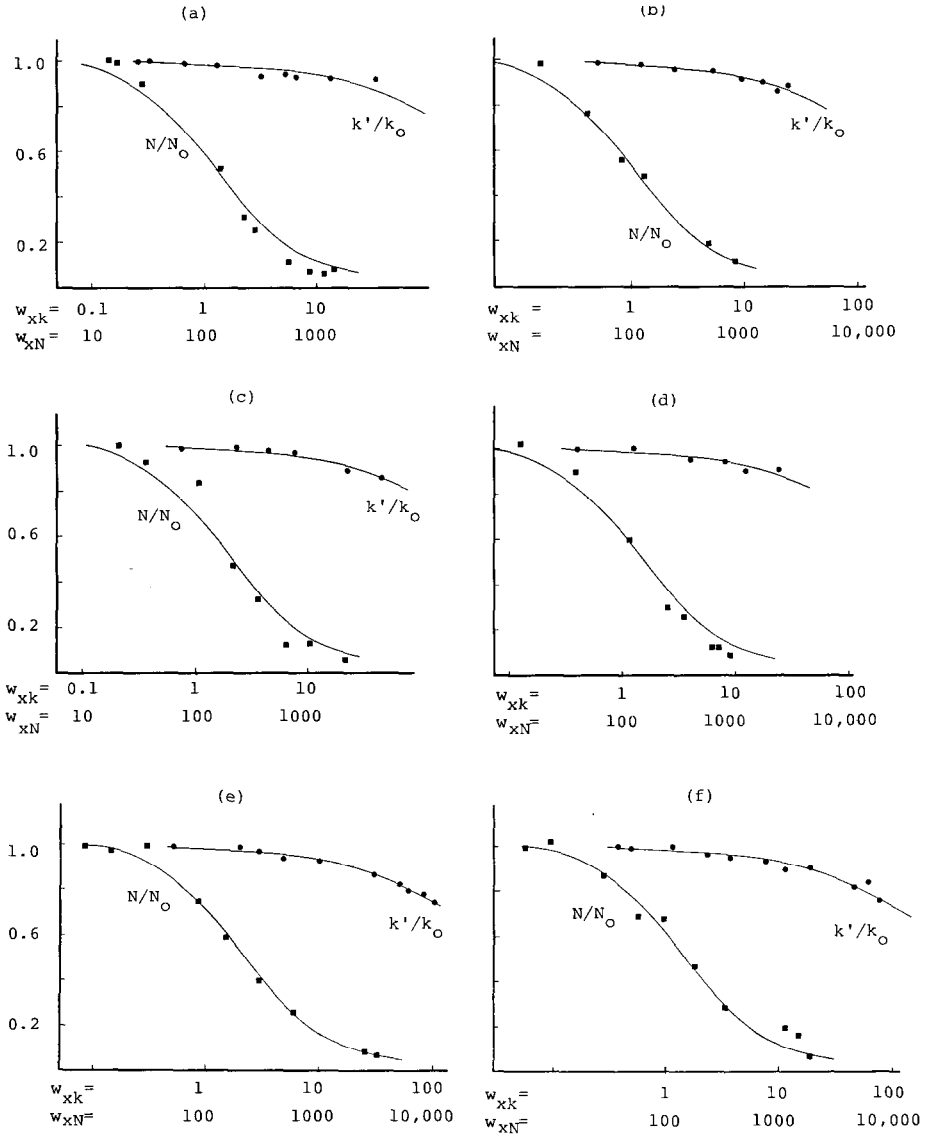

Fig. 24. Data of Figs. 6 and 7 replotted for particular values of flow-rate and mobile phase composition. (a) 20% (v/v) methanol, 0.89 ml/min; (b) 20%, 6.8 ml/min; (c) 30%, 0.89 ml/min; (d) 30%, 6.8 ml/min; (e) 40%, 0.89 ml/min; (f) 40%, 6.8 ml/min. (●) Data for k'/k_0; (■) data for N/N_0.

degree with flow-rate and mobile phase composition, but it is possible that these apparent differences are within experimental error.

Differences in chromatographic w_s values: k'/k_0 vs. N/N_0. The data in Table V show a consistent bias toward higher values of w_s from the k'/k_0 plots, compared to the corresponding N/N_0 plots: average ratio, 2.5; range, 1.3–4.5. We initially considered some possible causes for this discrepancy:

TABLE VI

EFFECT OF FLOW-RATE AND SOLVENT STRENGTH ON w_s VALUES FOR BENZYL ALCOHOL AND THE ZORBAX ODS COLUMN.

Data from Fig. 24.

Mobile phase (methanol–water)	w_s *(mg)*				
	0.89 ml/min		*6.8 ml/min*		*Average**
	k'/k_0	N/N_0	k'/k_0	N/N_0	
20:80	75	25	60	25	46
30:70	105	40	75	30	62
40:60	80	45	74	30	57
Average**:	62		49		

* Average value for each mobile phase.
** Average value for each flow-rate.

(i) transient overloading of the particle surface, with a greater effect on N than on k',

(ii) poor mass distribution of the sample at the column inlet,

(iii) viscosity effects from concentrated sample solutions.

"Transient overloading" refers to the fact that as a band passes a sorbent particle, the concentration (and stationary phase load) will be higher at the outside of the particle. The Craig model does not take such an effect into account. We would expect this to be more important at higher flow-rates, where the sample has less time to come to equilibrium with the interior of the particle. In this case, plots as in Figs. 6 and 7 should show that high-flow-rate data (solid points, 6.8 ml/min) are biased toward higher values of x in Fig. 6, and toward lower values of x in Fig. 7. That is, the discrepancy in apparent w_s values should increase for higher flow-rates, if this effect is responsible for the different w_s values from k' *vs.* N plots. However, no such tendencies are to be found in these data. This is confirmed by the data of Table VI, which show that the ratio of w_s values from k' *vs.* N plots is constant (2.4 ± 0.4) as the flow-rate is varied. We therefore consider transient overloading effects as unlikely.

Poor mass distribution of the sample across the column (in a radial direction) could occur during sample injection. Again, this is not anticipated by the Craig model, and might explain the discrepancy in w_s values. This possibility was investigated by repeating one of the above studies, but with a distributor plate installed at the column inlet to improve the sample distribution during injection. The system chosen was benzyl alcohol as solute, the Zorbax ODS column, and methanol–water (40:60) at 0.89 ml/min. Resulting plots of k'/k_0 and N/N_0, as in Figs. 6 and 7 showed no difference, with or without a distributor plate.

Finally, sample viscosity as a variable was investigated by comparing 15-μl injections of highly viscous benzyl alcohol solutions with 50-μl injections of a less concentrated (therefore less viscous) solution. The volumes of both injections were such as to have no effect on N_0. Again, no effect on derived values of w_s could be seen.

At the moment, we do not have an explanation for the larger w_s values in the case of k'/k_0 plots. However, we believe that the effect is real and consistent (for data in Tables V and VI, ratio = 2.5 ± 0.8, 1 S.D.; 14 systems). Meanwhile we will simply use this ratio as an empirical constant in further applications of our model for predictive purposes.

Measuring values of w_s

The present study is intended to facilitate the design of preparative HPLC separations, by allowing predictions of separation as a function of sample size and other conditions. This approach requires an estimate of the effective column capacity w_s. We have seen that values of w_s can be obtained, either from isotherm measurements (Table II), or from chromatographic runs (Table V) plus measurement of "cumulative"* values of k' and N. Practical workers will prefer to avoid either of these alternatives, since they involve additional work and tedious procedures. Therefore, in applying our model in practice, another approach to determining "effective" values of w_s would be advantageous. This is possible, simply by measuring "band" values of k' in the usual way, for sample injections in the overload region (*e.g.*, using a small-scale column). The resulting plots of k'/k_0 *vs.* w_{xk} w_s can be used to estimate w_s, in the same way as in Fig. 6 for "cumulative" values of k'/k_0. The corresponding master curve is shown in Fig. 5c and tabulated in Table III.

Fig. 25 shows four representative plots of "band" values of k'/k_0 *vs.* w_{xk}. The curves through each data set are predicted from w_{xk} values in Fig. 5c along with the w_s values in Table V (chromatographic values from k' plots). Good agreement is seen in all four cases. For all 9 sample–column systems tested, the values of w_s obtained from fitting the k'/k_0 "band" data to the master plot in Fig. 5c showed good agreement with the values in Table V. We therefore assume that w_s values obtained from "band" elution data can be related to values obtained from "cumulative" data. Consequently, values of w_s (for k'/k_0 predictions) can be obtained for any HPLC system, using the procedure of Fig. 25.

The theoretical approach of Poppe and Kraak[16] yields a prediction of N/N_0 *vs.* w_{xN} for columns that are not too severely overloaded:

$$w_x \text{ (for } N/N_0 = 0.9) = 2(1+k_0)^2 w_s/N_0\, k_0^2 \tag{9}$$

For a typical case from Tables III and V, we have for the benzyl alcohol–Zorbax ODS system: w_s = 60 mg, N_0 = 1800, k_0 = 2.9. Eqn. 9 predicts for this example that w_x = 120 μg should lead to a 10% decrease in N/N_0, whereas the experimental value is 35 μg. That is, the column overloads 3.5-fold faster than predicted. We have no explanation for this discrepancy, although it might be noted that this factor of 3.5 is similar to that found for experimental w_s values from N/N_0 *vs.* k'/k_0 plots (2.5-fold).

The preceding observation means that eqn. 9 appears to yield a 3.5-fold discrepancy when applied to the present experimental system (benzyl alcohol–Zorbax ODS). However the form of eqn. 9 correctly correlates values of N/N_0 *vs.* w_{xN}, as in

* "Cumulative" and "band" measurements of k' and N were discussed in ref. 1; (*cf.* Fig. 1 of ref. 1).

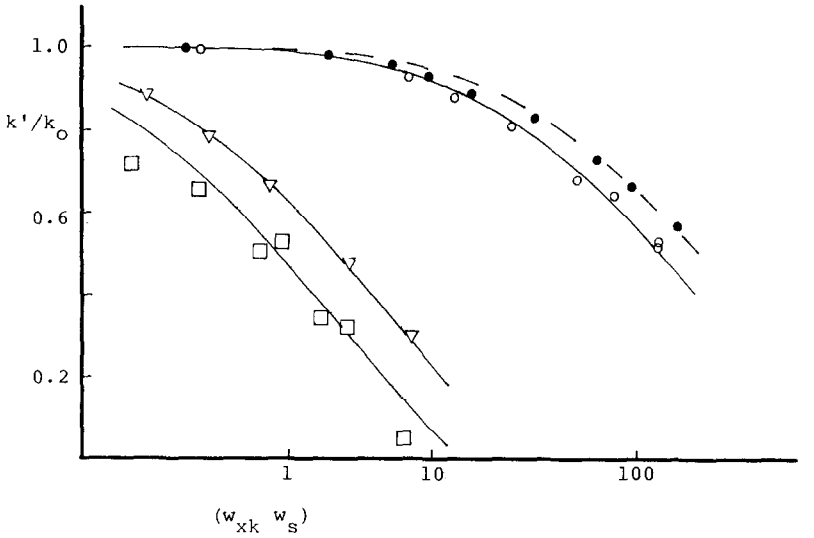

Fig. 25. Plots of "band" values of k'/k_0 *vs.* w_{xk} w_s for different solute–column conditions. (———) Calculated curves based on w_s values from "cumulative" k'/k_0 plots of Table V plus master curve of Fig. 5c. (●) Data for benzyl alcohol and Zorbax C_8 column; (○) data for benzyl alcohol and Zorbax 150-C_8 column; (▽) data for angiotensin II and ODS column; (□) data for insulin A chain and C_8 column.

TABLE VII

COLUMN CAPACITIES w_s (TOTAL COVERAGE) ON A mg/m² BASIS

Solute–column	*Pore diameter (nm)*	*Surface area (m²)**		*w_s/SA** (mg/m²)*
		Silica	*Bonded-phase*	
Benzyl alcohol–Zorbax ODS	6–7	200 m	110 m	0.55
Angiotensin II–Zorbax ODS	6–7	200	110	0.55
Caffeine–Zorbax C_8	10	600	530	0.22
7β-Hydroxypropyl-theophyline–Zorbax C_8	10	600	530	0.35
Benzyl alcohol–Zorbax C_8	10	200	178	0.56
Benzyl alcohol–Zorbax 150-C_8	15–17	84	78	0.91

* m²/column; silica values are experimentally determined; bonded-phase values calculated as described in text.

** Maximum w_s values for solute at large values of C_x; average of values of Table V from k'/k_0 and N/N_0 plots.

Fig. 7. Therefore any error in eqn. 9 has no effect on our present treatment (model simulation).

Column capacity values w_s as a function of pore diameter and surface area

Table VII summarizes (maximum) values of column capacity per unit surface (w_s/SA, mg/m^2) for the various systems of Table V. Eqn. 7 suggests that w_s/SA $\approx$ 0.3 mg/m^2, if the solute molecules are adsorbed in a flat configuration. It is seen (Table VII) that in all cases except for caffeine, this value is exceeded. This is expected, in that the adsorption of one monolayer of solute in a flat configuration yields a minimum surface capacity. For larger-pore-size packings (15–17 nm), w_s/SA $\approx$ 0.9 mg/m^2. That is, in this larger pore, the concentration of solute molecules sorbed on the stationary phase surface is 3-times greater than predicted by eqn. 7. Apparently, flat adsorption is not preferred in this case*. The uptake of organic solvent from reversed-phase solvent–water mobile phases has been reported equal to 2–4 monolayers[17], corresponding to w_s/SA values of 0.6–1.2 mg/m^2 (for wide-pore packings). This figure is reduced by 40% in 6-nm-pore packings[10], in agreement with the smaller w_s/SA values of Table VII for 6- to 10-nm-pore packings (0.2–0.6 mg/m^2) *vs.* 15- to 17-nm-pores (0.9 mg/m^2).

Jacobson *et al.*[13] have measured isotherms for several phenol and benzoic acid derivatives in a reversed-phase HPLC system (water as mobile phase). They found that these data follow the Langmuir isotherm over the range of C_x values studied (10 to 20-fold variation in C_x, *vs.* 100- to 1000-fold variation of C_x in our present studies). Values of w_s for this system can be determined[18], as summarized in Table VIII. These values of w_s/SA are generally lower than would be expected from Table VI for a 9-nm-pore packing (about 0.4 mg/m^2), and are quite variable. With water as mobile phase in this system, it is possible that the bonded-phase surface is sufficiently collapsed to prevent any penetration of solute molecules into the bonded phase. If so, the maximum column capacity should be given by eqn. 7; *i.e.*, 0.3 mg/m^2. The monofunctional phenols and anilines in fact have w_s/SA values in this range; *i.e.* 0.21–0.65 mg/m^2. The data in Table VI further support the proposal that values of w_s may be lower for water as mobile phase, in that a 20% reduction in w_s was observed for 20% (v/v) methanol compared to 30 or 40% methanol mobile phases (Table VI).

The much lower w_s/SA values for the benzoic acids of Table VIII probably arise from competitive adsorption of the ionized solute. That is, initially adsorbed solute molecules (carrying a negative charge) create a negative charge on the column-packing surface, and this discourages further sorption of negatively-charged sample molecules (note similar effects in ion-pairing; Fig. 4 of ref. 19). The solute *p*-aminobenzoic acid has a very low value of w_s/SA, similar to that for angiotensin II or insulin A chain in Table V. *p*-Aminobenzoic acid probably exists as the zwitterion, and it may be retained on silanols by cation exchange. If this is the case, w_s for this compound should be lower by about 2 orders of magnitude (*cf.* values of w_s in Table V), and this is roughly the case.

Resorcinol and hydroquinone have intermediate values of w_s/SA, which may reflect the presence of two strongly hydrogen-bonding groups in the molecule. These

* Alternatives to flat adsorption include vertical adsorption, which may involve partial penetration into the bonded phase, as well as an actual partitioning into the stationary phase.

TABLE VIII

VALUES OF w_s/SA FROM THE STUDY OF JACOBSON *et al.*[13]

C_{18}, 9-nm-pore column; water as mobile phase, buffered at pH = 6.3 for benzoic acid derivatives only.

Solute	w_s/SA *(mg/m²)**
Phenol	0.21
Resorcinol	0.09
Hydroquinone	0.03
m-Cresol	0.33
p-cresol	0.47
o-Toluidine	0.46
p-Toluidine	0.65
Benzoic acid	0.04
p-Aminobenzoic acid	0.004
m-Nitrobenzoic acid	0.05
2-Amino-4-nitrophenol	0.21

* Calculated from the bonded-phase surface area, assuming that this equals 0.72 times the silica surface area (220 m^2/g) (Table III).

probably prevent the molecule from penetrating the non-polar hydrocarbon phase, forcing flat-wise adsorption which then requires more surface area per molecule.

From the foregoing discussion it may be concluded that predicting values of w_s for a given reversed-phase system is at best uncertain. However, for uncharged molecules it appears that w_s will vary from 0.2 to 1.0 mg/m^2 of silica surface, being larger for wider-pore packings. Much lower values of w_s are possible, whenever silanols play a major role in sample retention and/or the solute molecule carries a charge.

Using the present model to predict the elution band

The data in Figs. 6–24 suggest that values of k' and N should be accurately predictable as a function of sample size, once values of k_0, N_0 and w_s have been determined. Since this is somewhat complicated, it is useful to summarize our predictive scheme in detail:

(i) Run initial chromatograms to obtain values of k_0 and N_0 (small sample, analytical-scale column).

(ii) Run 3–5 additional chromatograms (same column) with larger samples, such that k'/k_0 is decreased to about 0.9 or less.

(iii) Plot "band" values of k'/k_0 *vs.* $\{[k_0/(1+k_0)]\, N^{\frac{1}{2}} w_x\}$ and superimpose these data onto Fig. 5c (or values of Table IV) in order to determine w_s (band).

(iv) Cumulative values of w_s are given as 1.0 w_s (band) for k'/k_0; 0.4 w_s (band) for N/N_0.

(v) Use the values (iv) of w_s (cumulative) plus k_0 and N_0 to obtain values of k' and N from Fig. 5 (or Table IV).

(vi) With these values of k', N and w_s, predict the elution curve (as described in Appendix II of ref. 1) for the scaled-up separation (same packing), assuming that w_s is proportional to the column volume.

Examples of the prediction of actual elution curves are shown in Fig. 26 for benzyl alcohol and the 150-C_8 column. Sample sizes of 0.01–1.6 mg are used, resulting in large changes in the elution band. The experimental data points are seen to track the predicted elution curves closely, except for the 1.6-mg-run. N/N_0 for this run was predicted by our model to be about 0.08, while the actual experimental value was $N/N_0 = 0.05$. The present model appears to be less accurate for heavily overloaded columns.

A similar comparison for insulin A chain as solute and a C_8 column is shown in Fig. 27. The agreement between experimental and predicted elution curves is similar to that seen in Fig. 26.

CONCLUSION

The preceding paper presented a model for predicting elution bands under overload conditions. This model is based on a Craig-distribution process, with assumption of a Langmuir isotherm. In the present study we examined other isotherm types, both theoretically and experimentally. It appears that many HPLC isotherms fail to meet all the requirements for Langmuir sorption. For example, sorption sites of different types (or energy) can be present in the stationary phase, ionized solutes may exhibit competitive adsorption, etc.

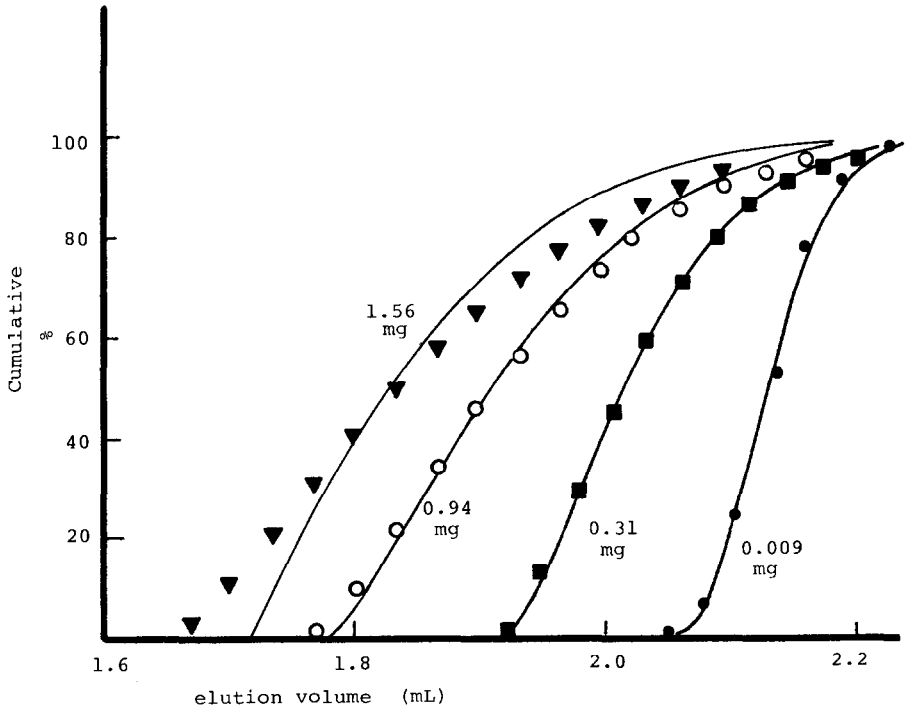

Fig. 26. Experimental *vs.* predicted elution curves for benzyl alcohol and Zorbax 150-C_8 column as a function of sample size. (———) Predicted curves as described in text. (●) Data points for 9.4 μg; (■) 314 μg; (○) 940 μg; (▼) 1560 μg.

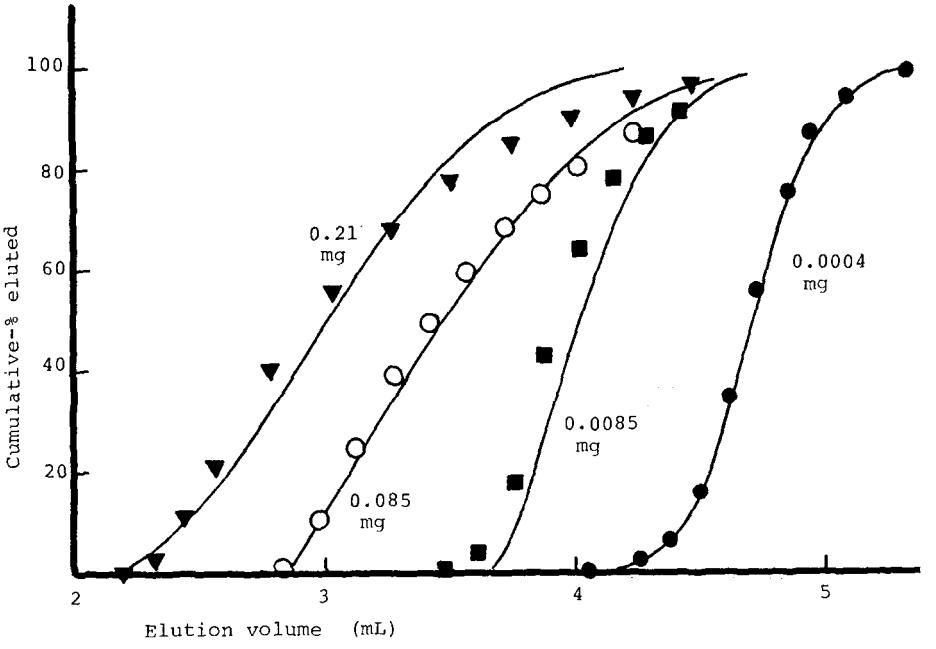

Fig. 27. Experimental *vs.* predicted elution curves for insulin A chain and Zorbax C_8 column as a function of sample size. (———) Predicted curves, as described in text. (●) Data points for 0.42 μg; (■) 8.5 μg; (○) 84.6 μg; (▼) 212 μg.

In many cases (including the Freundlich isotherm), these non-Langmuir isotherms closely resemble the Langmuir isotherm within a certain range of sample concentrations. Our model is then able to predict separation under overload conditions with reasonable accuracy. A general characteristic of these non-Langmuir systems is that the "apparent" column-saturation capacity w_s (as reflected in chromatographic performance at overload) is lower than the actual capacity of the column (as determined at high solute concentrations). We describe how the "apparent" w_s value for a given sample and column can be measured conveniently. Maximum values of the column capacity w_s occur for non-ionic samples (or for systems where silanol-retention effects are minimized).

Nine different reversed-phase systems were studied experimentally in an overload mode (5 solutes, 4 columns). Elution curves could be accurately predicted for these various experiments, using the present model. This provides a basis for extending our approach to the prediction of separations that involve two or more co-eluting solutes. This work is near completion and will be described within the near future.

APPENDIX I

Calculating the isotherm for the case of a large solute molecule displacing several small solvent molecules

The equilibrium constant K is related to mole fractions of X and M in the adsorbed (a) and liquid (m) phases as

$$K = N_{xa}\, N^n_{mm}/N_{xm}N^n_{ma} \approx N_{xa}/N_x N^n_{ma} \tag{A1}$$

Here N_{xa} refers to the mole fraction of solute X in the adsorbed phase (a), N_x is the mole fraction of X in the mobile phase, and N_{ma} is the mole fraction of mobile phase in the adsorbed phase. Eqn. A1 assumes that the mole fraction of solute in the mobile phase (N_x) is always small, which is a good approximation for most cases. If the densities of X and M are assumed equal, then the capacity factor k' can be expressed as

$$k' = \varphi\theta_x/C_x \tag{A2}$$

θ_x is the fraction of the surface covered by molecule X, C_x is the concentration (g/ml) of sample in the mobile phase, and φ is the phase ratio — equal to the weight of a monolayer of sample or mobile phase (assumed equal here) divided by the column dead volume V_m.

The mole fraction of X in the mobile phase N is given by

$$\begin{aligned} N &= (\text{moles X})/(\text{total moles}) \\ &= (C_x/M_x)/[C_x/M_x) + (C_s/M_s)] \\ &\approx C_x(M_s/M_x) = C_x/n \end{aligned} \tag{A3}$$

Eqn. A3 assumes that N_x (and C_x) is small, and that (M_x/M_m) is equal to n. In similar fashion we have

$$N_{xa} = (\theta_x/n)/[(\theta_x/n) + \theta_s] \tag{A4}$$

and

$$N_{sa} = \theta/[(\theta_x/n) + \theta_s] \tag{A5}$$

Beginning with values of θ_x, K, n and φ, a value of k' can be determined from the above relationships: $\theta_s = (1 - \theta_x)$, and N_{xa} and N_{sa} are determined from eqns. A4 and A5. These quantities are next substituted into eqn. A1 to obtain N_x. C_x is then calculated from N_x and eqn. A3.

REFERENCES

1 J. E. Eble, P. E. Antle, R. L. Grob and L. R. Snyder, *J. Chromatogr.*, 384 (1987) 25.
2 L. R. Snyder, *Principles of Adsorption Chromatography*, Marcel Dekker, New York, 1968.
3 L. R. Snyder and H. Poppe, *J. Chromatogr.*, 184 (1980) 363.
4 L. R. Snyder, in Cs. Horváth (Editor), *High-performance Liquid Chromatography. Advances and Perspectives*, Vol. 3, Academic Press, New York, 1983, p. 157.
5 M. Jaroniec, J. K. Różylo and W. Gołkiewicz, *J. Chromatogr.*, 178 (1979) 27.
6 W. Rudzinski and J. N-Michalek, *J. Chem. Soc., Faraday Trans. 1*, 81 (1985) 553.
7 X. Geng and F. E. Regnier, *J. Chromatogr.*, 296 (1984) 15.
8 X. Geng and F. E. Regnier, *J. Chromatogr.*, 332 (1985) 147.

9 J. P. Larman, J. J. DeStefano, A. P. Goldberg, R. W. Stout, L. R. Snyder and M. A. Stadalius, *J. Chromatogr.*, 255 (1983) 163.
10 M. A. Quarry, R. L. Grob and L. R. Snyder, *J. Chromatogr.*, 285 (1984) 19.
11 A. Tchapla, H. Colin and G. Guiochon, *Anal. Chem.*, 56 (1984) 621.
12 A. W. J. de Jong, J. C. Kraak, H. Poppe and F. Nooitgedacht, *J. Chromatogr.*, 193 (1980) 181.
13 J. Jacobson, J. Frenz and Cs. Horváth, *J. Chromatogr.*, 316 (1984) 53.
14 U. Lund, *J. Liq. Chromatogr.*, 4 (1981) 1933.
15 J. E. Eble, *Thesis*, Villanova University, Villanova, PA, 1986.
16 H. Poppe and J. C. Kraak, *J. Chromatogr.*, 255 (1983) 395.
17 N. Le Ha, J. Ungvaral and E. sz. Kovats, *Anal. Chem.*, 54 (1982) 2410.
18 Cs. Horváth, personal communication.
19 J. H. Knox and R. A. Hartwick, *J. Chromatogr.*, 204 (1981) 3.